WEAK FORMULATION AND FINITE ELEMENT APPROXIMATION OF THE NAVIER-STOKES EQUATION WITH FREE SURFACE

Emmanuel Audusse, Gabriel R Barrenechea, Astrid Decoene, Pierrick Quemar

WEAK FORMULATION AND FINITE ELEMENT APPROXIMATION OF THE NAVIER-STOKES EQUATION WITH FREE SURFACE

EMMANUEL AUDUSSE, GABRIEL R. BARRENECHEA, ASTRID DECOENE, AND PIERRICK QUEMAR

Abstract. In this work we study the numerical approximation of incompressible Navier-Stokes equations with free surface. The evolution of the free surface is driven by the kinematic boundary condition, and an Arbitrary Lagrangian Eulerian (ALE) approach is used to derive a weak formulation which involves three fields, namely, velocity, pressure, and the function describing the free surface. This formulation is discretised using finite elements in space and a time-advancing explicit finite difference scheme in time. In fact, the domain tracking algorithm is explicit: first, we solve the equation for the free surface, then move the mesh according to the sigma transform, and finally we compute the velocity and pressure in the updated domain. This explicit strategy is built in such a way that global conservation can be proven, which plays a pivotal role in the proof of stability of the discrete problem. The well-posedness and stability results are independent of the viscosity of the fluid, but while the proof of stability for the velocity is valid for all time steps, and all geometries, the stability for the free surface requires a CFL condition. The performance of the current approach is presented via numerical results and comparisons with the characteristics finite element method.

1. Introduction

Free surface flows appear in numerous applications, ranging from phase-change problems [31], through to coating flows [13], to glacier movement [26] and oceanographics and costal flows [17], to name just a few. From a mathematical point of view, the modelling of such problems changes depending on what the application requires. Sometimes surface tension is added, for example in small scale applications such as air bubbles in water (see, e.g., the discussion given in [27]), while for larger scale applications such as coastal flows the surface tension can be neglected (see, e.g. [17]). Regardless of the surface tension, the free surface can be described in terms of the *kinematic* boundary condition which, in essence, states that the free surface is advected according to the velocity of the fluid. This can be done in a completely explicit way, that is, by deforming the free surface according to the fluid velocity, or it can be done by solving a transport equation.

From qualitative partial differential equation perspective, the incompressible Navier-Stokes equation with free surface has been analysed in numerous papers, most of them considering infinite spatial domains, or periodic boundary conditions. In [3] local existence is proven for the problem considering surface tension and a transport equation for the free surface. The regularity issue for the transport problem describing the free surface is avoided in [35], where existence results are proven under milder conditions. Later, in [16] local existence results are proven neglecting the surface tension. In all these works, the fact the equation contains viscosity is of paramount importance, thus their results are not applicable to Euler's equation in a direct way. The fact that the solution of the Navier-Stokes equations with free surface tends to that of Euler's equation with free surface has only recently been proven in [22].

From a numerical perspective, solving the incompressible Navier-Stokes equation with free surface numerically using, e.g., finite element methods has been the topic of numerous studies, especially in the computational mechanics perspective, where a vast literature can be found, but mostly lacking a detailed numerical analysis. Other than the solution of the Navier-Stokes equation by itself, one main difficulty of the free surface problem lies in the fact that the computational mesh needs to change in time to be able to follow the evolution of the domain. It is a very well documented fact that the naive approach of remeshing at each time step is prohibitely expensive. So, alternative approaches need to be considered. For example, level set methods can be used in

conjunction with characteristics finite element methods as it has been done, e.g., in [21]. Alternatively, a *monolithic* approach can be followed, where a fully space-time problem is solved, see, e.g., [1] where some stability results are also obtained for a problem including surface tension.

One of the most popular approaches for flow problems on evolving domains is the Arbitrary Lagrangian Eulerian (ALE) approach [19, 30]. It consists in defining an arbitrary velocity of the domain that matches the deformation of its boundaries, allowing for a smooth update of the mesh at each time step. The finite element method for the ALE formulation of the free surface has been used in several works. For example, in [23] a characteristics finite element method is proposed, and analysed under the assumption that the discrete velocity is exactly divergence-free; in [10] a $\mathbb{P}_1 - \text{iso} - \mathbb{P}_2$ element is considered for the velocity while continuous piecewise linear elements were used for the pressure. Also, in [34, 12] stabilised finite element methods are used to approximate the Navier-Stokes equations with free surface. Despite the large number of papers devoted to solving the Navier-Stokes equation with free surface using an ALE formulation, up to our best knowledge, the papers addressing stability and convergence of the numerical schemes are not numerous. For example, in [24] and ALE finite element method is analysed for a convection-diffusion equation, while in [29] the analysis is performed for the linear Stokes equations in a moving domain.

The purpose of this work is to fill the gap hinted in the last paragraph. More precisely, we analyse a new finite element method for the Navier-Stokes equations with free surface, without surface tension. The problem's unknowns are velocity, pressure, and the position of the free surface, which is modelled by a transport equation arising from the kinematic condition. The starting point is to provide a weak formulation for this problem based on the use of the Sigma-ALE transform [8], and the writing of the convective term in its skew-symmetric way. While this weak formulation seems to be novel, it is closely related to the one used at the discrete level in [14], where an interface problem in MHD is considered. Once the weak formulation written, we present a finite element method and a mesh tracking strategy. The problem is solved in a decoupled explicit way, where we first approximate the evolution of the free surface by solving a stabilised finite element problem for the transport equation driving the free surface. Under an appropriate CFL condition it can be proven that the water depth remains positive, which is at the heart of the numerical strategy, as this allows us to define the deformed mesh. Then, as a second step a mesh modification is carried out based on the sigma transform, and finally, the Navier-Stokes equation is approximated in the deformed domain using the MINI element for the velocity and pressure. Stability results both for the fluid velocity, and for the free surface are given, under appropriate CFL conditions.

One important property of the present method, which plays a paramount role in the stability analysis, is the conservation of the water quantity, a property that is not shared by every numerical method (in fact, our numerical experiments show that the characteristics method does not preserve the water quantity). Moreover, if the problem is solved in an explicit way by advecting the free surface without solving a transport equation, as done in [12], then a careful choice for the normal vectors needs to be made in order to ensure global conservation (see, e.g., [37]). Up to our best knowledge, no stability analysis has been done for this latter approach. One possible reason for this lack of analysis is that advecting the free surface by the velocity can be recast as an explicit solution of an unstabilised transport equation, while in the stability analysis presented below the stabilisation term was of paramount importance to prove stability of the free surface.

The rest of the manuscript is organised as follows. The rest of this first section is devoted to present some notations that will be used throughout and the problem of interest. The weak formulation of the problem is derived in Section 2. The finite element method is presented in Section 3, where its conservativity, well-posedness, and stability are proven. Finally, in Section 4 we present the results of numerous simulations in two- and three-dimensional benchmark problems.

1.1. **Notation and the problem of interest.**

Let us first introduce some notations. We will use standard notation for Lebesgue and Sobolev spaces, aligned, e.g., with [11], and [15]. For a general domain Ω, $W^{s,p}(\Omega)$ denotes the Sobolev space of real-valued functions defined on the

domain Ω with distributional derivatives of order up to $s \in \mathbb{N}$ that belong to $L^p(\Omega)$. The associated norm is $\|\cdot\|_{s,p,\Omega}$ and the seminorm is $|\cdot|_{s,p,\Omega}$. In the case where $s = 0$, we obtain the Lebesgue space $W^{0,p}(\Omega) = L^p(\Omega)$. The case $p = 2$ will be distinguished by using the Hilbert space $W^{s,2}(\Omega) = H^s(\Omega)$. For simplicity, we denote respectively by $\|\cdot\|_{s,\Omega}$ and $|\cdot|_{s,\Omega}$ the norm and the seminorm in $H^s(\Omega)$. In the case, $s = 0, p = 2$, the inner product of $L^2(\Omega)$ is denoted by $(\cdot,\cdot)_\Omega$ and the corresponding norm by $\|\cdot\|_{0,\Omega}$. The norm of the space of essentially bounded functions $L^\infty(\Omega)$ is denoted by $\|\cdot\|_{\infty,\Omega}$. For the sake of simplicity, for a moving domain Ω_t, we use the following notation: $(\cdot,\cdot)_t = (\cdot,\cdot)_{\Omega_t}$ and the corresponding norm is: $\|\cdot\|_{0,t} = \|\cdot\|_{0,\Omega_t}$. The norm of the space of essentially bounded functions $L^\infty(\Omega_t)$ is denoted by $\|\cdot\|_{\infty,t}$. Finally, we do not make a distinction between norms and inner products of scalar, and vector/tensor-valued functions.

We denote by ∇ the three-dimensional gradient operator and by $\nabla_{\rm hor}$ the two-dimensional gradient operator such that for all $f : \mathbb{R}^3 \to \mathbb{R}$ and for all $g : \mathbb{R}^2 \to \mathbb{R}$:

$$\nabla f = \left(\frac{\partial f}{\partial x}, \frac{\partial f}{\partial y}, \frac{\partial f}{\partial z}\right), \ \nabla_{\rm hor}\, g = \left(\frac{\partial g}{\partial x}, \frac{\partial g}{\partial y}\right). \tag{1}$$

Furthermore, we denote the three-dimensional divergence operator by div , such that for all $\mathbf{f} = (f_1, f_2, f_3) : \mathbb{R}^3 \to \mathbb{R}^3$

$$\operatorname{div} \mathbf{f} = \frac{\partial f_1}{\partial x} + \frac{\partial f_2}{\partial y} + \frac{\partial f_3}{\partial z}\,. \tag{2}$$

Over a period of time $[0, T]$, we consider a homogeneous, Newtonian fluid occupying a domain that varies with time. To define the domain, we consider the following ingredients: a

- ω: a fixed two-dimensional domain;
- $\Gamma_b := \{(x, y, b(x, y)) : (x, y) \in \omega\}$: the bottom of the domain; and
- $\Gamma_{s,t} := \{\big(x, y, \eta(t, (x, y))\big) : (x, y) \in \omega\}$: the free surface.

So, at any time t, the domain Ω_t is given by

$$\Omega_t = \left\{(x, y, z) \mid (x, y) \in \omega \text{ and } b(x, y) < z < \eta\big(t, (x, y)\big)\right\}\,, \tag{3}$$

where

- ω is a fixed two-dimensional domain;
- $\Gamma_b := \{(x, y, b(x, y)) : (x, y) \in \omega\}$ is the bottom of the domain; and
- $\Gamma_{s,t} := \left\{\big(x, y, \eta(t, (x, y))\big) : (x, y) \in \omega\right\}$ is the free surface.

For simplicity we will suppose that ω is a polygon, and that Γ_b is a polyhedral surface. The boundary of Ω_t is then given by $\partial\Omega_t = \Gamma_{s,t} \cup \Gamma_{l,t} \cup \Gamma_b$, where $\Gamma_{l,t}$ is the *lateral* boundary, considered to be impervious. We denote by $\boldsymbol{n}$ the unit outward normal vector on $\partial\Omega_t$. We distinguish between the unit normal on the boundary, and the normal vector to the free boundary $\Gamma_{s,t}$ given by

$$\boldsymbol{n}_{s,t} = (-\nabla\eta(t, (x, y)), 1)^T\,, \tag{4}$$

so $\boldsymbol{n} = \frac{1}{\|\boldsymbol{n}_{s,t}\|}\boldsymbol{n}_{s,t}$ on $\Gamma_{s,t}$. The fluid's velocity is denoted by $\boldsymbol{u} = (u, v, w)$ and its pressure is denoted p. The horizontal component of the velocity (u, v) is denoted by $\boldsymbol{u}^{\rm hor}$. At the free surface $\Gamma_{s,t}$, these velocities are respectively denoted by $\boldsymbol{u}^{\rm hor}_{|_{z=\eta}}$ and $w_{|_{z=\eta}}$.

Throughout we will denote the physical time space domain

$$\mathcal{S} = \cup_{t\in(0,T)} \left\{(t, \boldsymbol{x}),\ \boldsymbol{x} \in \Omega_t\right\}. \tag{5}$$

We will consider a fluid with constant density $\rho = 1$ for simplicity, although computations are made with $\rho = 1000$ kg/m^3. Assuming that the only volumetric force is the gravity given by $\mathbf{g} = -g\,\mathbf{e}_z$ and neglecting the surface tension, the fluid motion in Ω_t is governed by the incompressible Navier-Stokes equations:

$$\frac{\partial \boldsymbol{u}}{\partial t} + (\boldsymbol{u} \cdot \nabla)\boldsymbol{u} - \operatorname{div} \sigma(\boldsymbol{u}, p) = \mathbf{g}, \qquad \text{in } \mathcal{S}\,, \tag{6}$$

$$\operatorname{div} \boldsymbol{u} = 0, \qquad \text{in } \mathcal{S}\,, \tag{7}$$

where

$$\sigma(\boldsymbol{u},p) = 2\nu\mathbb{D}(\boldsymbol{u}) - p\mathbf{I}, \qquad \mathbb{D}(\boldsymbol{u}) = \frac{1}{2}\left(\nabla\boldsymbol{u} + \nabla\boldsymbol{u}^T\right),$$

are the total stress and the strain tensors, respectively, and ν is the kinematic viscosity (supposed constant throughout this manuscript). These equations are completed with the following boundary conditions:

$$\sigma(\boldsymbol{u},p)\boldsymbol{n} = \mathbf{0}, \quad \text{on } \Gamma_{s,t}, \tag{8}$$

$$\boldsymbol{u}\cdot\boldsymbol{n} = 0, \quad \text{on } \Gamma_b \cup \Gamma_{l,t}, \tag{9}$$

$$(\sigma(\boldsymbol{u},p)\boldsymbol{n})\cdot\mathbf{t} = 0, \quad \text{on } \Gamma_b \cup \Gamma_{l,t}, \tag{10}$$

and the following kinematic condition at the free surface

$$\frac{\partial\eta}{\partial t} = \boldsymbol{u}|_{z=\eta}\cdot\boldsymbol{n}_{s,t} \quad \text{in } \omega\,. \tag{11}$$

Relation (8) is a dynamic boundary condition at the free surface expressing the continuity of the normal stress; notice that we have considered a constant atmospheric pressure chosen to be $p_{atm} = 0$. Equalities (10) and (9) are, respectively, a dynamic and a kinematic boundary condition at the lateral boundaries and at the bottom, modelling slip-conditions. Note that the present work can be extended in a straightforward way to the case of friction conditions.

Finally, the kinematic condition (11) reflects the fact that fluid particles on the free surface remain at the surface. This choice guarantees the global conservation of the water quantity, and will be exploited at the discrete level. Due to the expression (4) for the normal vector on $\Gamma_{s,t}$, the kinematic condition can be rewritten as follows :

$$\frac{\partial\eta}{\partial t} + \boldsymbol{u}^{\text{hor}}_{|_{z=\eta}}\cdot\nabla_{\text{hor}}\eta = w_{|_{z=\eta}} \quad \text{in } \omega\,. \tag{12}$$

In order to contruct our numerical method, (12) is the form of the kinematic condition we will use. Nevertheless, we will keep in mind the formulation (11) as well.

Finally, the initial conditions for η and $\boldsymbol{u}$ are given by

$$\eta(t=0) = \eta^0 \quad \text{in } \omega \quad \text{and} \quad \boldsymbol{u}(t=0) = \boldsymbol{u}_0 \quad \text{in } \Omega_0\,, \tag{13}$$

where $\boldsymbol{u}_0$ is divergence-free and satisfies (9).

1.2. **The ALE framework.** Our numerical strategy is based on a moving mesh that remains conformal to the free surface at each time step. For that purpose, we use the Arbitrary Lagrangian Eulerian (ALE) approach, which allows for an arbitrary choice of the mesh movement inside the fluid domain. The approach can be formulated by defining a fixed reference domain denoted by $\widehat{\Omega}$ and a time dependent mapping between $\widehat{\Omega}$ and the moving physical domain. We choose $\widehat{\Omega} = \omega\times(0,1)$, although it could for instance be given by the initial domain. We consider that the domain only moves in the vertical direction; this movement can be arbitrarily defined in the interior but it must match the movement of the physical boundaries. We define it by means of the following family of "ALE–Sigma" mappings (see for instance [8]) :

$$\begin{aligned} \mathcal{A} : \mathbb{R}^+\times\widehat{\Omega} &\mapsto \mathbb{R}^3 \\ (t,\widehat{\boldsymbol{x}}) &\mapsto \boldsymbol{x} = (\hat{x},\hat{y},Z(t,\widehat{\boldsymbol{x}}))\,, \end{aligned}$$

where $\widehat{\boldsymbol{x}} = (\hat{x},\hat{y},\hat{z})$ and Z is a continuous and monotonic function ($\partial Z/\partial z > 0$) satisfying $Z(t,(\hat{x},\hat{y},0)) = b(\hat{x},\hat{y})$ and $Z(t,(\hat{x},\hat{y},1)) = \eta(t,(\hat{x},\hat{y}))$, the latter two conditions ensuring that $\mathcal{A}(t,\widehat{\Omega}) = \Omega_t$ for all $t \geq 0$. A simple and classical choice for the function Z is the so-called sigma transform [17, 33, 25], which has been widely used in the atmospheric and oceanographic communities and is defined as follows :

$$Z\big(t,(\hat{x},\hat{y},\hat{z})\big) = \big[\eta(t,(\hat{x},\hat{y})) - b(\hat{x},\hat{y})\big]\,\hat{z} + b(\hat{x},\hat{y}). \tag{14}$$

We denote $\mathcal{A}_t = \mathcal{A}(t,\cdot)$ the mapping which at time $t \geq 0$ associates a point $\widehat{\boldsymbol{x}} \in \widehat{\Omega}$ to a point $\boldsymbol{x} \in \Omega_t$. We define the velocity of the domain, denoted by $\boldsymbol{c}$, as follows:

(15)
$$\mathbf{c}(t,\boldsymbol{x}) = \frac{\partial \mathcal{A}}{\partial t}\left(t, \mathcal{A}_t^{-1}(\boldsymbol{x})\right) = \left(0, 0, \frac{\partial Z}{\partial t}\left(t, \mathcal{A}_t^{-1}(\boldsymbol{x})\right)\right)^T = \left(0, 0, \frac{z - b(x,y)}{\eta(t,x,y) - b(x,y)} \frac{\partial \eta}{\partial t}(t,x,y)\right)^T.$$

Remark 1.1. *It is worth remarking that the definition* (15) *of the mesh velocity* $\boldsymbol{c}$*, together with the kinematic condition* (11) *imply that* $\boldsymbol{u}$ *and* $\boldsymbol{c}$ *are linked as follows:*

$$\mathbf{c} \cdot \boldsymbol{n} = \boldsymbol{u} \cdot \boldsymbol{n} \qquad \text{on the physical boundaries of the domain.} \tag{16}$$

This is the classical consistency condition for an ALE mapping, ensuring that $\Omega_t = \mathcal{A}(t, \widehat{\Omega})$ *for all* $t \geq 0$*.*

We introduce the following standard definition of the ALE time derivative

$$\left.\frac{\partial \boldsymbol{u}}{\partial t}\right|_{\widehat{\Omega}}(t,\boldsymbol{x}) = \frac{\partial \widehat{\boldsymbol{u}}}{\partial t}\left(t, \mathcal{A}_t^{-1}(\boldsymbol{x})\right), \quad \text{where } \widehat{\boldsymbol{u}}(t,\widehat{\boldsymbol{x}}) = \boldsymbol{u}(t, \mathcal{A}_t(\widehat{\boldsymbol{x}})) \text{ for } \widehat{\boldsymbol{x}} \in \widehat{\Omega}, \tag{17}$$

and recall the following relation

$$\frac{\partial \boldsymbol{u}}{\partial t}(t,\boldsymbol{x}) = \left.\frac{\partial \boldsymbol{u}}{\partial t}\right|_{\widehat{\Omega}}(t,\boldsymbol{x}) - (\mathbf{c}(t,\boldsymbol{x}) \cdot \nabla)\boldsymbol{u}(t,\boldsymbol{x}). \tag{18}$$

With the above notations and assumptions, we derive the following strong form of the free surface Navier–Stokes equations in the ALE framework:

$$\left.\frac{\partial \boldsymbol{u}}{\partial t}\right|_{\widehat{\Omega}} + \big((\boldsymbol{u} - \mathbf{c}) \cdot \nabla\big)\boldsymbol{u} - \operatorname{div} \sigma(\boldsymbol{u}, p) = \mathbf{g}, \qquad \text{in } \mathcal{S}\,, \tag{19}$$

$$\operatorname{div} \boldsymbol{u} = 0, \qquad \text{in } \mathcal{S}\,, \tag{20}$$

$$\frac{\partial \eta}{\partial t} + \boldsymbol{u}^{\text{hor}}_{|_{z=\eta}} \cdot \nabla_{\text{hor}}\, \eta = w_{|_{z=\eta}}, \quad \text{on } (0,T) \times \omega\,, \tag{21}$$

with boundary conditions (8), (9), and (10).

2. The weak formulation

In this Section, we introduce a weak formulation of the free surface Navier–Stokes equations (19)-(21). Using the ALE mapping $\mathcal{A}_t$ we define the spaces where the velocity and pressure are sought

$$\mathcal{V}(t,\Omega_t) = \{\boldsymbol{v} : \mathcal{S} \to \mathbb{R}^3,\ \boldsymbol{v}(t,\cdot) = \widehat{\boldsymbol{v}}(t,\cdot) \circ \widehat{\mathcal{A}}_t^{-1},\ \widehat{\boldsymbol{v}}(t,\cdot) \in H^1(\widehat{\Omega})^3\}, \tag{22}$$

$$\mathcal{V}_0(t,\Omega_t) = \{\boldsymbol{v} \in \mathcal{V}(t,\Omega_t),\ \boldsymbol{v}(t,\cdot) \cdot \boldsymbol{n} = 0 \text{ on } \Gamma_b \cup \Gamma_{l,t}\ \forall t \in (0,T)\}, \tag{23}$$

$$\mathcal{Q}(t,\Omega_t) = \{q : \mathcal{S} \to \mathbb{R},\ q(t,\cdot) = \widehat{q}(t,\cdot) \circ \widehat{\mathcal{A}}_t^{-1},\ \widehat{q}(t,\cdot) \in L^2(\widehat{\Omega})\}. \tag{24}$$

The spaces for the test functions are defined in a quasi-static way, for each $t \in (0,T)$, as follows:

$$\mathcal{V}(\Omega_t) = \{\boldsymbol{v} : \Omega_t \to \mathbb{R}^3,\ \boldsymbol{v} = \widehat{\boldsymbol{v}} \circ \widehat{\mathcal{A}}_t^{-1},\ \widehat{\boldsymbol{v}} \in H^1(\widehat{\Omega})^3\}, \tag{25}$$

$$\mathcal{V}_0(\Omega_t) = \{\boldsymbol{v} \in \mathcal{V}(\Omega_t),\ \boldsymbol{v} \cdot \boldsymbol{n} = 0 \text{ on } \Gamma_b \cup \Gamma_{l,t}\}, \tag{26}$$

$$\mathcal{Q}(\Omega_t) = \{q : \Omega_t \to \mathbb{R},\ q = \widehat{q} \circ \widehat{\mathcal{A}}_t^{-1},\ \widehat{q} \in L^2(\widehat{\Omega})\}. \tag{27}$$

The functional space for the free surface is defined on ω and given by:

$$\mathcal{N}(\omega) = L^\infty((0,T), L^2(\omega)) \cap L^2((0,T), H^1(\omega)). \tag{28}$$

With these spaces for the velocity, pressure, and free surface, we introduce the weak formulation to be used throughout: Find $(\boldsymbol{u}, p, \eta) \in \mathcal{V}_0(t,\Omega_t) \times \mathcal{Q}(t,\Omega_t) \times \mathcal{N}(\omega)$ such that for all $(\boldsymbol{v}, q, \psi) \in$

$\mathcal{V}_0(\Omega_t) \times \mathcal{Q}(\Omega_t) \times H^1(\omega)$ and almost all $t \in (0,T)$ the following holds

$$\frac{d}{dt}(\boldsymbol{u},\boldsymbol{v})_t + a(\boldsymbol{u},\boldsymbol{v}) + \overline{c}(\boldsymbol{u}-\mathbf{c},\boldsymbol{u},\boldsymbol{v}) - \frac{1}{2}(\boldsymbol{u}\,\mathrm{div}\,\mathbf{c},\boldsymbol{v})_t - b(\boldsymbol{v},p) = (\mathbf{g},\boldsymbol{v})_t, \tag{29}$$

$$-b(\boldsymbol{u},q) = 0, \tag{30}$$

$$\Big(\frac{\partial \eta}{\partial t},\psi\Big)_\omega + (\boldsymbol{u}^{\mathrm{hor}}_{|_{z=\eta}} \cdot \nabla\eta,\psi)_\omega = (w_{|_{z=\eta}},\psi)_\omega, \tag{31}$$

where the forms $a(\cdot,\cdot), b(\cdot,\cdot)$ and $\overline{c}(\cdot;\cdot,\cdot)$ are defined by

$$a(\boldsymbol{u},\boldsymbol{v}) = 2\nu\left(\mathbb{D}(\boldsymbol{u}),\mathbb{D}(\boldsymbol{v})\right)_t, \tag{32}$$

$$b(\boldsymbol{v},q) = (\mathrm{div}\,\boldsymbol{v},q)_t\,, \tag{33}$$

$$\overline{c}(\boldsymbol{u}-\mathbf{c},\boldsymbol{u},\boldsymbol{v}) = \frac{1}{2}\Big[\Big(\big((\boldsymbol{u}-\mathbf{c})\cdot\nabla\big)\boldsymbol{u},\boldsymbol{v}\Big)_t - \Big(\big((\boldsymbol{u}-\mathbf{c})\cdot\nabla\big)\boldsymbol{v},\boldsymbol{u}\Big)_t\Big]. \tag{34}$$

One salient feature of this weak problem is the antisymmetry of the form $\overline{c}(\cdot;\cdot,\cdot)$, namely $\overline{c}(\boldsymbol{u}-\mathbf{c},\boldsymbol{u},\boldsymbol{v}) = -\overline{c}(\boldsymbol{u}-\mathbf{c},\boldsymbol{v},\boldsymbol{u})$. This property facilitates the stability analysis greatly (see also [14] where a finite element method based on a similar rewriting of the convective term was derived in the MHD context). So, in the next result we justify the fact (29)-(31) is a valid weak formulation.

Theorem 2.1. *The weak problem* (29)-(31) *is a weak formulation for the free surface Navier-Stokes equation* (19)-(21)*.*

Proof. We multiply each equation in (19)-(21) by a test function and integrate on the corresponding space domain. After integration by parts we obtain the following standard weak form : *Find* $(\boldsymbol{u},p) \in \mathcal{V}_0(t,\Omega_t) \times \mathcal{Q}(t,\Omega_t)$ *and* $\eta \in \mathcal{N}(\omega)$ *such that for all* $(\boldsymbol{v},q) \in \mathcal{V}_0(\Omega_t) \times \mathcal{Q}(\Omega_t)$*,* $\psi \in H^1(\omega)$ *and for almost all* $t \in (0,T)$

$$\int_{\Omega_t} \frac{\partial \boldsymbol{u}}{\partial t}\Big|_{\widehat{\Omega}} \cdot \boldsymbol{v}\,\mathrm{d}\boldsymbol{x} + c(\boldsymbol{u}-\mathbf{c},\boldsymbol{u},\boldsymbol{v}) + a(\boldsymbol{u},\boldsymbol{v}) - b(\boldsymbol{v},p) = (\mathbf{g},\boldsymbol{v})_t, \tag{35}$$

$$-b(\boldsymbol{u},q) = 0, \tag{36}$$

$$\Big(\frac{\partial \eta}{\partial t},\psi\Big)_\omega + (\boldsymbol{u}^{\mathrm{hor}}_{|_{z=\eta}} \cdot \nabla\eta,\psi)_\omega = (w_{|_{z=\eta}},\psi)_\omega\,, \tag{37}$$

where the convective form $c(\cdot,\cdot,\cdot)$ is given by

$$c(\boldsymbol{u}-\mathbf{c},\boldsymbol{u},\boldsymbol{v}) = \Big(\big((\boldsymbol{u}-\mathbf{c})\cdot\nabla\big)\boldsymbol{u},\boldsymbol{v}\Big)_t.$$

Then, we use the Reynolds Transport Theorem (see, e.g., [28]) and the fact that the ALE time derivative of the test function $\boldsymbol{v}$ is zero, to write :

$$\int_{\Omega_t} \frac{\partial \boldsymbol{u}}{\partial t}\Big|_{\widehat{\Omega}} \cdot \boldsymbol{v}\,\mathrm{d}\boldsymbol{x} = \int_{\Omega_t} \frac{\partial(\boldsymbol{u}\cdot\boldsymbol{v})}{\partial t}\Big|_{\widehat{\Omega}}\,\mathrm{d}\boldsymbol{x} = \int_{\Omega_t} \frac{\partial(\boldsymbol{u}\cdot\boldsymbol{v})}{\partial t} + \mathbf{c}\cdot\nabla(\boldsymbol{u}\cdot\boldsymbol{v})\,\mathrm{d}\boldsymbol{x} \tag{38}$$

$$= \frac{d}{dt}\int_{\Omega_t} \boldsymbol{u}\cdot\boldsymbol{v}\,\mathrm{d}\boldsymbol{x} - \int_{\Omega_t} (\boldsymbol{u}\cdot\boldsymbol{v})\,\mathrm{div}\,\mathbf{c}\,\mathrm{d}\boldsymbol{x}. \tag{39}$$

Replacing (39) in (35) leads to

$$\frac{d}{dt}(\boldsymbol{u},\boldsymbol{v})_t + c(\boldsymbol{u}-\mathbf{c},\boldsymbol{u},\boldsymbol{v}) - (\boldsymbol{u}\,\mathrm{div}\,\mathbf{c},\boldsymbol{v})_t + a(\boldsymbol{u},\boldsymbol{v}) - b(\boldsymbol{v},p) = (\mathbf{g},\boldsymbol{v})_t. \tag{40}$$

Next, the convective term $c(\cdot,\cdot,\cdot)$ can be rewritten as follows:

$$c(\boldsymbol{u}-\mathbf{c},\boldsymbol{u},\boldsymbol{v}) = \frac{1}{2}\Big[\Big(\big((\boldsymbol{u}-\mathbf{c})\cdot\nabla\big)\boldsymbol{u},\boldsymbol{v}\Big)_t + \Big(\big((\boldsymbol{u}-\mathbf{c})\cdot\nabla\big)\boldsymbol{u},\boldsymbol{v}\Big)_t\Big]. \tag{41}$$

Integrating by parts on the second term leads to:

$$c(\boldsymbol{u}-\mathbf{c},\boldsymbol{u},\boldsymbol{v}) = \overline{c}(\boldsymbol{u}-\mathbf{c},\boldsymbol{u},\boldsymbol{v}) + \frac{1}{2}\big((\boldsymbol{u}-\mathbf{c})\cdot\boldsymbol{n},\boldsymbol{u}\cdot\boldsymbol{v}\big)_{\partial\Omega_t} - \frac{1}{2}\Big(\boldsymbol{u}\,\mathrm{div}\,(\boldsymbol{u}-\mathbf{c}),\boldsymbol{v}\Big)_t. \tag{42}$$

Thus, using the last equality, $\boldsymbol{u}\cdot\boldsymbol{n} = \boldsymbol{c}\cdot\boldsymbol{n}$ (cf. Remark 1.1) on $\partial\Omega_t$ and the fact that $\boldsymbol{u}$ is divergence-free, the convective term finally reads

$$c(\boldsymbol{u}-\mathbf{c},\boldsymbol{u},\boldsymbol{v}) = \overline{c}(\boldsymbol{u}-\mathbf{c},\boldsymbol{u},\boldsymbol{v}) + \frac{1}{2}\Big(\boldsymbol{u}\,\mathrm{div}\,\mathbf{c},\boldsymbol{v}\Big)_t. \tag{43}$$

Replacing (43) in (40) shows that (29) is a rewriting of (35). This concludes the proof. □

3. The finite element method

In this section we present the finite element method for the weak problem (29)-(31). Besides presenting the overall numerical strategy, we also prove global conservation and stability results.

The time interval $(0,T)$ is divided into N time steps of length $\Delta t \in \mathbb{R}^+$, and denote $t^n = t^{n-1} + \Delta t$ for $n = 1,\dots,N$ (we do not suppose that the time step Δt is constant in time, but we keep the notation Δt to avoid unnecessary complications). We denote by $(\boldsymbol{u}_h^n, p_h^n, \eta_h^n)$ the approximation of $(\boldsymbol{u}, p, \eta)$ at the time t^n (these will belong to finite element spaces defined below).

In this work, we have chosen to decouple the deformation of the domain and the fluid approximation, and then we adopt the following explicit numerical strategy to track the evolution of the free surface: given $(\boldsymbol{u}_h^n, p_h^n, \eta_h^n)$, then

i/ advect the free surface in order to compute η_h^{n+1};
ii/ update the discrete domain to Ω_h^{n+1} through the ALE mapping;
iii/ compute the approximate velocity and pressure $(\boldsymbol{u}_h^{n+1}, p_h^{n+1})$ on the updated domain.

We start defining the finite element spaces in the reference domain $\widehat{\Omega}$, and in ω. Let $\mathcal{P}_\mathfrak{h}$ be a quasi-uniform simplicial triangulation of the horizontal domain ω, made up of triangles of diameter at most $\mathfrak{h}$, and let $\widehat{\mathcal{T}}_h$ be the triangulation of the reference domain obtained by piling up the horizontal mesh on N_z layers on the vertical from $\hat{z}=0$ to $\hat{z}=1$, and then dividing each resulting prism into 3 tetrahedra. In $\widehat{\mathcal{T}}_h$ we define the lowest order mini-element (see [15]), that is, if for a simplex $K \subseteq \mathbb{R}^3$ we define the standard quartic bubble function b_K, the finite element spaces for velocity and pressure are given by

$$\widehat{\mathcal{V}}_h(\widehat{\Omega}) = \Big\{\widehat{\boldsymbol{v}}_h \in C^0\big(\overline{\widehat{\Omega}}\big)^3 : \widehat{\boldsymbol{v}}_h|_{\widehat{K}} \in \Big(\mathbb{P}_1(\widehat{K}) \oplus \mathrm{span}\{b_{\widehat{K}}\}\Big)^3,\ \text{for all } \widehat{K} \in \widehat{\mathcal{T}}_h\Big\}, \tag{44}$$

$$\widehat{\mathcal{Q}}_h(\widehat{\Omega}) = \{\widehat{q}_h \in C^0(\overline{\widehat{\Omega}}) : \widehat{q}_h|_{\widehat{K}} \in \mathbb{P}_1(\widehat{K}),\ \text{for all } \widehat{K} \in \widehat{\mathcal{T}}_h\}. \tag{45}$$

In addition η is approximated in the following finite element space

$$\mathcal{N}_\mathfrak{h}(\omega) = \{\psi_\mathfrak{h} \in C^0(\omega) : \psi_\mathfrak{h}|_\kappa \in \mathbb{P}_1(\kappa)\ ,\ \forall \kappa \in \mathcal{P}_\mathfrak{h}\}. \tag{46}$$

The space $\mathcal{N}_\mathfrak{h}(\omega)$ is independent of time, and provides a description of the free surface, as at the time t^n the free boundary $\Gamma_{h,s}^n$ is given in terms of the finite element approximation of η, denoted by η_h^n. Using η_h^n we define the following discrete ALE mapping $\mathcal{A}_{h,n} : \widehat{\Omega} \mapsto \mathbb{R}^3$ defined as follows:

$$(x,y,z) = \mathcal{A}_{h,n}(\hat{\boldsymbol{x}}) \ = \ \big(\hat{x},\hat{y},(\eta_h^n(\hat{x},\hat{y}) - b(\hat{x},\hat{y}))\,\hat{z} + b(\hat{x},\hat{y})\big). \tag{47}$$

We thus define the approximated domain

$$\Omega_h^n = \mathcal{A}_{h,n}(\widehat{\Omega}). \tag{48}$$

Notice that the discrete domain Ω_h^n (defined using the approximated free surface η_h^n) does not coincide with Ω_{t^n} (defined using the free surface $\eta(t^n,.)$). The discrete boundary of the domain Ω_h^n is denoted $\partial\Omega_h^n$ and the discrete free surface part is $\Gamma_{h,s}^n$, then $\partial\Omega_h^n = \Gamma_{h,s}^n \cup \Gamma_{h,l}^n \cup \Gamma_b$. The corresponding norm is, by an abuse of notation, denoted by $\|\cdot\|_{0,n}$, and the discrete inner product on the discrete domain Ω_h^n is denoted by $(\cdot,\cdot)_{h,n}$.

Using the mapping $\mathcal{A}_{h,n}$ we also build the corresponding triangulation $\mathcal{T}_h^n$ of the domain Ω_h^n

$$\mathcal{T}_h^n = \Big\{\mathcal{A}_{h,n}(\hat{K})\ /\ \hat{K} \in \widehat{\mathcal{T}}_h\Big\}. \tag{49}$$

The elements belonging to $\mathcal{T}_h^n$ have diameters at most h. We will distinguish between h (the three-dimensional diameter of the tetrahedron), and $\mathfrak{h}$ only when it is needed. Since the ALE mapping

$\mathcal{A}_{h,n}$ is affine inside each element of the triangulation $\widehat{\mathfrak{T}}_h$, the elements of $\mathfrak{T}_h^n$ are simplices not containing any hanging nodes as the time advances.

On the mesh $\mathfrak{T}_h^n$ and using the discrete ALE mapping $\mathcal{A}_{h,n}$ we define the finite element spaces for velocity and pressure by

$$\mathcal{V}_h(\Omega_h^n) = \{\boldsymbol{v}_h^n : \Omega_h^n \to \mathbb{R}^3,\ \boldsymbol{v}_h^n = \widehat{\boldsymbol{v}}_h \circ \widehat{\mathcal{A}}_{h,n}^{-1},\ \widehat{\boldsymbol{v}}_h \in \widehat{\mathcal{V}}_h(\widehat{\Omega})\}, \tag{50}$$

$$\mathcal{V}_{h,0}(\Omega_h^n) = \{\boldsymbol{v}_h^n \in \mathcal{V}_h(\Omega_h^n)^3 \mid \boldsymbol{v}_h^n \cdot \boldsymbol{n} = 0 \text{ on } \Gamma_b \cup \Gamma_{h,l}^n\}, \tag{51}$$

$$\mathcal{Q}_h(\Omega_h^n) = \{q_h^n : \Omega_h^n \to \mathbb{R},\ q_h^n = \widehat{q}_h \circ \widehat{\mathcal{A}}_{h,n}^{-1},\ \widehat{q}_h \in \widehat{\mathcal{Q}}_h(\widehat{\Omega})\}. \tag{52}$$

It is a well-known fact (see, e.g., [15]) that these spaces satisfy the discrete inf-sup condition

$$\inf_{q_h^n \in \mathcal{Q}_h(\Omega_h^n)} \sup_{\boldsymbol{v}_h^n \in \mathcal{V}_h(\Omega_h^n)} \frac{(\operatorname{div} \boldsymbol{v}_h^n, q_h^n)}{\|\boldsymbol{v}_h^n\|_{1,n}\|q_h^n\|_{0,n}} \geq \beta_0^n, \tag{53}$$

with $\beta_0^n > 0$ for all $n \in \{0, \dots, N\}$. Even if we do not assume a uniform lower bound for β_0^n, (53) ensures that (58)-(59), introduced below, is well-posed.

Remark 3.1. *Reading carefully the proof of the inf-sup condition for the MINI-element given in, e.g.,* [15]*, we can deduce that $\beta_0^n > 0$, even if it might degenerate if the mesh $\mathfrak{T}_h^n$ becomes anisotropic (e.g., if the water depth becomes very small). This is, in any case, not a limitation for the proof of well-posedness of the problem, and for the stability results proven below.*

With the previous definitions, we now describe the numerical strategy proposed in this work. We start with the initial conditions. The initial condition η_h^0 is chosen as the Lagrange interpolant of η^0. As initial condition for the velocity we choose the Riesz projection of $\boldsymbol{u}_0$; that is, we choose as $\boldsymbol{u}_h^0$ the unique solution of: find $(\boldsymbol{u}_h^0, \chi_h) \in \mathcal{V}_{h,0}(\Omega_h^0) \times \mathcal{Q}_h(\Omega_h^0)$ such that

$$(\nabla \boldsymbol{u}_h^0, \nabla \boldsymbol{v}_h)_{h,0} - (\chi_h, \operatorname{div} \boldsymbol{v}_h)_{h,0} = (\nabla \boldsymbol{u}_0, \nabla \boldsymbol{v}_h)_{h,0} \qquad \forall\, \boldsymbol{v}_h \in \mathcal{V}_{h,0}(\Omega_h^0)\,, \tag{54}$$

$$(\xi_h, \operatorname{div} \boldsymbol{u}_h^0)_{h,0} = 0 \qquad \forall\, \xi_h \in \mathcal{Q}_h(\Omega_h^0)\,. \tag{55}$$

Once the initial conditions are given, we detail each of the steps of our decoupled strategy.

- For the first step, we discretize in time and space the problem (31) for the free surface using a first order forward Euler scheme in time and the space $\mathcal{N}_{\mathfrak{h}}(\omega)$. That is, we solve the following problem: Find $\eta_h^{n+1} \in \mathcal{N}_{\mathfrak{h}}(\omega)$ such that for all $\zeta_h \in \mathcal{N}_{\mathfrak{h}}(\omega)$ the following holds

$$\left(\frac{\eta_h^{n+1} - \eta_h^n}{\Delta t}, \zeta_h\right)_\omega + \left(\boldsymbol{u}_{h|_{z=\eta_h^n}}^{n,\mathrm{hor}} \cdot \nabla \eta_h^n, \zeta_h\right)_\omega + s_h^n(\eta_h^n, \zeta_h) = \left(w_{h|_{z=\eta_h^n}}^n, \zeta_h\right)_\omega, \tag{56}$$

  where the stabilization term is given by

$$s_h^n(\eta_h^n, \zeta_h) = \frac{\mathfrak{h}}{\left\|\boldsymbol{u}_{h|_{z=\eta_h^n}}^{n,\mathrm{hor}}\right\|_{\infty,\omega}} \left(\boldsymbol{u}_{h|_{z=\eta_h^n}}^{n,\mathrm{hor}} \cdot \nabla \eta_h^n, \boldsymbol{u}_{h|_{z=\eta_h^n}}^{n,\mathrm{hor}} \cdot \nabla \zeta_h\right)_\omega. \tag{57}$$

- The second step reduces to define the mesh and the finite element spaces on the new domain Ω_h^{n+1} using the discrete ALE mapping as in (47)-(52).
- The third (and final) stage consists in solving the following discrete problem for the velocity and pressure: Find $(\boldsymbol{u}_h^{n+1}, p_h^{n+1}) \in \mathcal{V}_{h,0}^{n+1}(\Omega_h^{n+1}) \times \mathcal{Q}_h^{n+1}(\Omega_h^{n+1})$ such that for all $(\boldsymbol{v}_h, q_h) \in \mathcal{V}_{h,0}^{n+1}(\Omega_h^{n+1}) \times \mathcal{Q}_h^{n+1}(\Omega_h^{n+1})$ the following holds

$$\begin{aligned}(\boldsymbol{u}_h^{n+1}, \boldsymbol{v}_h)_{h,n+1} - (\boldsymbol{u}_h^n, \boldsymbol{v}_{h,n}^{n+1})_{h,n} + \Delta t \left[\overline{c}_{n+1}(\boldsymbol{u}_{h,n+1}^n - \mathbf{c}_{h,n+1}^n, \boldsymbol{u}_h^{n+1}, \boldsymbol{v}_h)\right.\\ \left. -\frac{1}{2}(\boldsymbol{u}_h^{n+1} \operatorname{div} \mathbf{c}_{h,n+1}^n, \boldsymbol{v}_h)_{h,n+1} + a_{n+1}(\boldsymbol{u}_h^{n+1}, \boldsymbol{v}_h) - b_{n+1}(\boldsymbol{v}_h, p_h^{n+1})\right] = (\mathbf{g}, \boldsymbol{v}_h)_{h,n+1},\end{aligned} \tag{58}$$

$$-b_{n+1}(\boldsymbol{u}_h^{n+1}, q_h) = 0, \tag{59}$$

  where the multilinear forms $a_{n+1}(\cdot,\cdot)$, $b_{n+1}(\cdot,\cdot)$ and $\overline{c}_{n+1}(\cdot,\cdot,\cdot)$ are the corresponding multilinear forms of (32), (33) and (34) on Ω_h^{n+1}, respectively. For two time steps t^m and

t^ℓ, and a function f defined in Ω_h^ℓ, we denote $f_m^\ell = f \circ \mathcal{A}_{h,\ell} \circ \mathcal{A}_{h,m}^{-1}$; that is, the function *transported* to the domain Ω_h^m. So, in (58)-(59) we have, in particular

$$\boldsymbol{v}_{h,n}^{n+1} = \boldsymbol{v}_h \circ \mathcal{A}_{h,n+1} \circ \mathcal{A}_{h,n}^{-1} \quad , \quad \boldsymbol{u}_{h,n+1}^{n} = \boldsymbol{u}_h^n \circ \mathcal{A}_{h,n} \circ \mathcal{A}_{h,n+1}^{-1} \,. \tag{60}$$

Using a discrete version of (15), the discrete mesh velocity $\mathbf{c}_{h,n+1}^n$ is defined on the domain Ω_h^{n+1} by

$$\mathbf{c}_{h,n+1}^n = \left(0, 0, \frac{\eta_h^{n+1} - \eta_h^n}{\Delta t} \frac{z - b}{\eta_h^{n+1} - b}\right) , \tag{61}$$

which is the way it is implemented in (58).

Remark 3.2. *It is worth mentioning that one fundamental requirement on the scheme is the fact that η_h^{n+1} needs to be strictly larger than b in order to define the deformed domain and mesh (cf. the definition* (47) *of the ALE mapping). Assuming that the initial condition η^0 satisfies $\eta^0 > b$, then up to choosing the time step Δt small enough, we can always assume that $\eta_h^{n+1} > b$ for every $n = 0, ..., N-1$. More precisely, we start noticing that* (56) *can be rewritten in the following equivalent way*

$$\left(\eta_h^{n+1} - \eta_h^n, \zeta_h\right)_\omega = \Delta t \left\{ (\boldsymbol{u}_{h|_{z=\eta_h^n}}^n \cdot \boldsymbol{n}_h^n, \zeta_h)_\omega - s_h^n(\eta_h^n, \zeta_h) \right\} , \tag{62}$$

for all $\zeta_h \in \mathcal{N}_{\mathfrak{h}}(\omega)$. Let now $\Phi_h \in \mathcal{N}_{\mathfrak{h}}(\omega)$ as the unique solution of

$$(\Phi_h, \zeta_h)_\omega = \left(\boldsymbol{u}_{h|_{z=\eta_h^n}}^n \cdot \boldsymbol{n}_h^n, \zeta_h \right)_\omega - s_h^n(\eta_h^n, \zeta_h) \,, \tag{63}$$

for all $\zeta_h \in \mathcal{N}_{\mathfrak{h}}(\omega)$. Then, (62) *and* (63) *lead to the following (pointwise) expression for η_h^{n+1}:*

$$\eta_h^{n+1}(x,y) - b(x,y) = \eta_h^n(x,y) - b(x,y) + \Delta t\, \Phi_h(x,y) \qquad \forall\, (x,y) \in \omega \,. \tag{64}$$

Let $\mathscr{N}$ be the set of nodes (x_i, y_i) of the mesh $\mathcal{P}_{\mathfrak{h}}$ where $\Phi_h(x_i, y_i) < 0$. Then, if we assume that

$$\Delta t < \min_{(x_i,y_i)\in\mathscr{N}} \frac{\eta_h^n(x_i,y_i) - b(x_i,y_i)}{-\Phi_h(x_i,y_i)} \,, \tag{65}$$

then, if $\eta^n > b$ in ω, thanks to (64) *we have that $\eta_h^{n+1} > b$ in ω. It is interesting to notice that* (65) *is fully computable, as the solution of* (63) *requires only the inversion of a the mass matrix of $\mathcal{N}_{\mathfrak{h}}(\omega)$, which is, in terms of computational cost, negligeable in comparison to the deformation of the domain and the computation of the updated velocity. So, from now on we assume that the time step Δt satisfies* (65).

We start showing that the discrete problem (58)-(59) is well-posed. We stress that since the equation (56) for η_h^{n+1} is an explicit formula relying only on the inversibility of the mass matrix, then proving that the velocity problem is well-posed gives us an immediate uniqueness result for the free surface.

Proposition 3.3. *The discrete variational form* (58)-(59) *is well-posed.*

Proof. Thanks to the discrete inf-sup stability of the mini-element the proof reduces to showing that the bilinear form

$$\begin{aligned} A(\boldsymbol{u}_h^{n+1}, \boldsymbol{v}_h) = (\boldsymbol{u}_h^{n+1}, \boldsymbol{v}_h)_{h,n+1} + \Delta t \big[\overline{c}_{n+1}(\boldsymbol{u}_{h,n+1}^n - \mathbf{c}_{h,n+1}^n, \boldsymbol{u}_h^{n+1}, \boldsymbol{v}_h) \\ - \frac{1}{2}(\boldsymbol{u}_h^{n+1} \mathrm{div}\, \mathbf{c}_{h,n+1}^n, \boldsymbol{v}_h)_{h,n+1} + a_{n+1}(\boldsymbol{u}_h^{n+1}, \boldsymbol{v}_h) \big], \end{aligned}$$

is elliptic. For this we study its three componenents separately. First, $a_{n+1}(\cdot,\cdot)$ is an elliptic bilinear form thanks to the Körn and Poincaré inequalities (see [11, Theorem 42.10] and [11, Lemma 3.27], respectively). In addition, for every $\boldsymbol{v} \in H^1(\Omega)^d$ we have

$$\overline{c}_h^{n+1}(\boldsymbol{u}_{h,n+1}^n - \mathbf{c}_{h,n+1}^n, \boldsymbol{v}, \boldsymbol{v}) = 0 \,.$$

So, to prove the ellipticity of $A(\cdot,\cdot)$ it only remains to show that

$$1 - \frac{\Delta t}{2}\mathrm{div}\,\mathbf{c}^n_{h,n+1} \geq 0. \tag{66}$$

Definition (61) for $\mathbf{c}^n_{h,n+1}$ gives

$$1 - \frac{\Delta t}{2}\mathrm{div}\,\mathbf{c}^n_{h,n+1} \geq \frac{\frac{\eta_h^{n+1}+\eta_h^n}{2} - b}{\eta_h^{n+1} - b} \geq 0\,, \tag{67}$$

thus proving the ellipticity of $A(\cdot,\cdot)$, and finishing the proof. □

3.1. **Mass conservation of the water quantity.** This section is devoted to proving that the sequence of approximations for the free surface generated by (56) preserves the global mass conservation. This is equivalent to stating that, once the initial approximation for η^0 has been chosen, the volume of the discrete domain remains constant in time, that is, $|\Omega_h^n| = |\Omega_h^{n-1}| = \cdots = |\Omega_h^0|$.

Proposition 3.4. *Let $\eta_h^{n+1} \in \mathcal{N}_{\mathfrak{h}}(\omega)$ be a solution of* (56)*. For all $n \in \mathbb{N}$, we have the following global mass conservation result:*

$$\int_\omega \eta_h^{n+1}\, d\omega = \int_\omega \eta_h^0\, d\omega\,. \tag{68}$$

As a consequence $|\Omega_h^n| = |\Omega_h^{n-1}| = \cdots = |\Omega_h^0|$.

Proof. Taking $\zeta_h = 1 \in \mathcal{N}_h(\omega)$ in (56) we arrive at

$$\frac{(\eta_h^{n+1},1)_\omega - (\eta_h^n,1)_\omega}{\Delta t} + \left(\boldsymbol{u}^{n,\mathrm{hor}}_{h|_{z=\eta_h^n}} \cdot \nabla\eta_h^n, 1\right)_\omega = \left(w^n_{h|_{z=\eta_h^n}}, 1\right)_\omega. \tag{69}$$

Defining the change of variable

$$\mathrm{d}\Gamma^n_{h,s} = \|\boldsymbol{n}^n_{h,s}\|\,\mathrm{d}\omega = \sqrt{1 + |\nabla_{\mathrm{hor}}\,\eta_h^n|^2}\,\mathrm{d}\omega\,, \tag{70}$$

between ω and $\Gamma^n_{h,s}$, (69) can be rewritten as follows:

$$\frac{(\eta_h^{n+1},1)_\omega - (\eta_h^n,1)_\omega}{\Delta t} = \int_{\Gamma^n_{h,s}} \boldsymbol{u}^n_{h|_{z=\eta_h^n}} \cdot \frac{\boldsymbol{n}^n_{h,s}}{\|\boldsymbol{n}^n_{h,s}\|}\mathrm{d}\Gamma^n_{h,s}\,. \tag{71}$$

Using that $\boldsymbol{u}_h^n \cdot \boldsymbol{n} = 0$ on $\partial\Omega_h^n \setminus \Gamma^n_{h,s}$ (71) becomes

$$\frac{(\eta_h^{n+1},1)_\omega - (\eta_h^n,1)_\omega}{\Delta t} = \int_{\partial\Omega_h^n} \boldsymbol{u}_h^n \cdot \boldsymbol{n}\,\mathrm{d}S\,. \tag{72}$$

The Gauss theorem and the fact that $\boldsymbol{u}_h^n$ satisfies (59) and $1 \in \mathcal{Q}_h(\Omega_h^n)$ yield

$$\frac{(\eta_h^{n+1},1)_\omega - (\eta_h^n,1)_\omega}{\Delta t} = \int_{\Omega_h^n} \mathrm{div}\,\boldsymbol{u}_h^n \mathrm{d}\boldsymbol{x} = b(\boldsymbol{u}_h^n, 1) = 0\,, \tag{73}$$

which concludes the proof. □

Remark 3.5. *The above result justifies our choice to approximate the free surface using an explicit method. In fact, for the conservation result to hold it is essential that in the right-hand side of* (71) *the normal vector and the velocity are defined at the same time step, in order to be able to use the discrete incompressibility condition on $\boldsymbol{u}_h^n$.*

3.2. **Stability estimate on the velocity field.** In this section we provide a stability result for the discrete velocity. Its proof relies on two preliminary results. The first one is a simplified Geometric Conservation Law (GCL) whose proof can be found in [7], while the second one is a discrete Gronwall inequality, proved originally in [18].

Lemma 3.6. *Let $f : \mathcal{S} \to \mathbb{R}$ be a regular function. Then*

$$\int_{\Omega_h^{n+1}} f^{n+1}\, d\boldsymbol{x} - \int_{\Omega_h^n} f_n^{n+1}\, d\boldsymbol{x} = \Delta t \int_{\Omega_h^{n+1}} f^{n+1} \mathrm{div}\, \mathbf{c}_{h,n+1}^n\, d\boldsymbol{x}\,. \tag{74}$$

Note that this is a discrete counterpart of the following continuous equation, valid for any regular function f :

$$\frac{d}{dt}\int_{\Omega_t} f\,\mathrm{d}\boldsymbol{x} = \int_{\Omega_t} \left.\frac{\partial f}{\partial t}\right|_{\widehat{\Omega}} \mathrm{d}\boldsymbol{x} + \int_{\Omega_t} f\,\mathrm{div}\,\mathbf{c}\,\mathrm{d}\boldsymbol{x}.$$

The discrete counterpart is ensured whenever the domain velocity $\mathbf{c}$ has a zero horizontal component.

Lemma 3.7. *Let $k, B, a_j, b_j, c_j, \gamma_j$, $j = 0, \ldots, n$, be nonnegative numbers such that*

$$a_n + k\sum_{j=0}^{n} b_j \le k\sum_{j=0}^{n} \gamma_j a_j + k\sum_{j=0}^{n} c_j + B, \quad \textit{for} \quad n \ge 0.$$

Suppose that $k\gamma_j < 1$, for all j, and set $\sigma_j = (1 - k\gamma_j)^{-1}$. Then

$$a_n + k\sum_{j=0}^{n} b_j \le \exp\left(k\sum_{j=0}^{n}\sigma_j\gamma_j\right)\left\{k\sum_{j=0}^{n} c_j + B\right\}, \quad \textit{for} \quad n \ge 0. \tag{75}$$

With these tools we now present the main result for stability of the velocity.

Theorem 3.8. *Let $\boldsymbol{u}_h^n$ be the solution of* (58)-(59)*. Then, for every $m \in \{0, \ldots, N\}$ the following stability holds for all $\Delta t < \frac{1}{2}$*

$$\|\boldsymbol{u}_h^m\|_{0,m}^2 + \Delta t \sum_{n=1}^{m} a_n(\boldsymbol{u}_h^n, \boldsymbol{u}_h^n) \le e^{2T}\left(\|\boldsymbol{u}_h^0\|_{0,0}^2 + g^2 T|\Omega_h^0|\right). \tag{76}$$

Proof. We consider $\boldsymbol{v}_h = \boldsymbol{u}_h^{n+1}$ in (58) to get to

$$\begin{aligned}(\boldsymbol{u}_h^{n+1}, \boldsymbol{u}_h^{n+1})_{h,n+1} - (\boldsymbol{u}_h^n, \boldsymbol{u}_{h,n}^{n+1})_{h,n} - \frac{\Delta t}{2}(\boldsymbol{u}_h^{n+1}\mathrm{div}\,\mathbf{c}_{h,n+1}^n, \boldsymbol{u}_h^{n+1})_{h,n+1}\\ + \Delta t\, a_{n+1}(\boldsymbol{u}_h^{n+1}, \boldsymbol{u}_h^{n+1}) = \Delta t\,(\mathbf{g}, \boldsymbol{u}_h^{n+1})_{h,n+1}.\end{aligned} \tag{77}$$

Applying the Cauchy–Schwarz and Young inequalities we get:

$$\begin{aligned}\|\boldsymbol{u}_h^{n+1}\|_{0,n+1}^2 - \frac{1}{2}\|\boldsymbol{u}_h^n\|_{0,n}^2 - \frac{1}{2}\|\boldsymbol{u}_{h,n}^{n+1}\|_{0,n}^2 - \frac{\Delta t}{2}(\boldsymbol{u}_h^{n+1}\mathrm{div}\,\mathbf{c}_{h,n+1}^n, \boldsymbol{u}_h^{n+1})_{h,n+1}\\ + \Delta t\, a_{n+1}(\boldsymbol{u}_h^{n+1}, \boldsymbol{u}_h^{n+1}) \le \Delta t\,\|\mathbf{g}\|_{0,n+1}\,\|\boldsymbol{u}_h^{n+1}\|_{0,n+1}.\end{aligned} \tag{78}$$

Next, to treat the term involving the divergence of the mesh velocity we apply (74) with $f = |\boldsymbol{u}_h^{n+1}|^2$ and get to

$$-\frac{\Delta t}{2}(\boldsymbol{u}_h^{n+1}\mathrm{div}\,\mathbf{c}_{h,n+1}^n, \boldsymbol{u}_h^{n+1})_{h,n+1} = -\frac{1}{2}\|\boldsymbol{u}_h^{n+1}\|_{0,n+1}^2 + \frac{1}{2}\|\boldsymbol{u}_{h,n}^{n+1}\|_{0,n}^2\,, \tag{79}$$

which, once inserted in (78) leads to:

$$\frac{1}{2}\|\boldsymbol{u}_h^{n+1}\|_{0,n+1}^2 - \frac{1}{2}\|\boldsymbol{u}_h^n\|_{0,n}^2 + \frac{\Delta t}{2}\,a_{n+1}(\boldsymbol{u}_h^{n+1}, \boldsymbol{u}_h^{n+1}) \le \frac{\Delta t}{2}\,\|\mathbf{g}\|_{0,n+1}^2 + \frac{\Delta t}{2}\,\|\boldsymbol{u}_h^{n+1}\|_{0,n+1}^2\,. \tag{80}$$

Using the discrete mass conservation (68) the first term in the right-hand side above becomes

$$\|\mathbf{g}\|_{0,n+1}^2 = \int_{\Omega_h^{n+1}} |\mathbf{g}|^2\,\mathrm{d}\boldsymbol{x} = g^2\,|\Omega_h^{n+1}| = g^2\,|\Omega_h^0|\,, \tag{81}$$

and then (80) becomes

$$\|\boldsymbol{u}_h^{n+1}\|_{0,n+1}^2 - \|\boldsymbol{u}_h^n\|_{0,n}^2 + \Delta t\, a_{n+1}(\boldsymbol{u}_h^{n+1}, \boldsymbol{u}_h^{n+1}) \leq \Delta t\, g^2\, |\Omega_h^0| + \Delta t\, \|\boldsymbol{u}_h^{n+1}\|_{0,n+1}^2 .$$

Finally, adding for $n = 0, \ldots, m-1$ we get

$$\|\boldsymbol{u}_h^m\|_{0,m}^2 + \Delta t \sum_{n=1}^{m} a_n(\boldsymbol{u}_h^n, \boldsymbol{u}_h^n) \leq \|\boldsymbol{u}_h^0\|_{0,0}^2 + g^2 T |\Omega_h^0| + \Delta t \sum_{n=1}^{m} \|\boldsymbol{u}_h^n\|_{0,n}^2 , \tag{82}$$

and the proof follows using the discrete Gronwall's inequality given in Lemma 3.7 with $\gamma_j = 1$, $c_j = 0$, $k = \Delta t$, and $B = \|\boldsymbol{u}_h^0\|_{0,0}^2 + g^2 T |\Omega_h^0|$. □

Remark 3.9. *It is important to mention that the above stability result was obtained without any assumption on the shape of the domain Ω_h^n or the regularity of the triangulation $\mathcal{T}_h^n$. In fact, Green's formulas require the domain to be Lipschitz, but this does not imply that the family $\{\Omega_h^n\}$ needs to be uniformily Lipschitz. In addition, the global conservation of the water quantity Lemma 3.4 was of paramount importance. Finally, we remark that this stability result is independent of the fluid viscosity, which explains why the present numerical strategy also provides satisfactory results in the inviscid case.*

Finally, in the absence of gravity ($g = 0$), we obtain the following energy estimate, reminiscent of [14, Proposition 3]*:*

$$\|\boldsymbol{u}_h^{n+1}\|_{0,n+1}^2 \leq \|\boldsymbol{u}_h^n\|_{0,n}^2 \qquad \text{for } n = 0, 1, 2, \ldots .$$

3.3. **Stability estimate on the free surface.** In this section we show the stability of the approximation for the free surface given by (56). Throughout this section we will suppose that the time step satisfies, in addition to (65), the following CFL conditions: There exists a constant $\alpha_0 > 0$ small enough such that

$$\Delta t \leq \frac{\alpha_0}{\|\boldsymbol{u}_h^n|_{z=\eta_h^n}\|_{\infty,\omega}} \mathfrak{h} . \tag{83}$$

In addition, we impose the following *inverse* CFL condition: There exists $\tilde{C} > 0$, independent of $\mathfrak{h}$ and Δt, but having the right physical units, such that

$$\mathfrak{h}^2 \leq \tilde{C}\, \Delta t . \tag{84}$$

One technical result we will use is the following: since the mesh $\mathcal{P}_\mathfrak{h}$ is quasi-uniform, the following global inverse inequality holds (see, e.g., [11, Ch. 12]): there exists $c_{\text{inv}} > 0$ such that

$$|\psi_\mathfrak{h}|_{1,\omega} \leq c_{\text{inv}} \mathfrak{h}^{-1} \|\psi_\mathfrak{h}\|_{0,\omega} \qquad \forall\, \psi_\mathfrak{h} \in \mathcal{N}_\mathfrak{h}(\omega) . \tag{85}$$

Lemma 3.10. *Let us suppose that the CFL condition* (83) *holds with a constant α_0 such that*

$$\alpha_0 \leq \frac{1}{4(1 + c_{\text{inv}}^2)} ,$$

where c_{inv} is the constant in the inverse inequality (85)*. Then, the following bound holds for $\eta_h^n \in \mathcal{N}_\mathfrak{h}(\omega)$, the solution of* (56)

$$\|\eta_h^{n+1} - \eta_h^n\|_{0,\omega}^2 \leq \; \Delta t \left[2\, \Delta t\, \|w_{h|_{z=\eta_h^n}}^n\|_{0,\omega}^2 + s_h^n(\eta_h^n, \eta_h^n) \right] . \tag{86}$$

Proof. We take $\zeta_h = \eta_h^{n+1} - \eta_h^n$ in (56) to obtain

$$\|\eta_h^{n+1} - \eta_h^n\|_{0,\omega}^2 = \Delta t \left[\left(w_{h|_{z=\eta_h^n}}^n, \eta_h^{n+1} - \eta_h^n\right)_\omega - \left(\boldsymbol{u}_{h|_{z=\eta_h^n}}^{n,\text{hor}} \cdot \nabla \eta_h^n, \eta_h^{n+1} - \eta_h^n\right)_\omega \right]$$

$$- \Delta t\, s_h^n(\eta_h^n, \eta_h^{n+1} - \eta_h^n) , \tag{87}$$

and using the Cauchy–Schwarz's inequality gives

$$\|\eta_h^{n+1} - \eta_h^n\|_{0,\omega}^2 \leq \Delta t\, \|\eta_h^{n+1} - \eta_h^n\|_{0,\omega} \left[\|w_{h|_{z=\eta_h^n}}^n\|_{0,\omega} + \|\boldsymbol{u}_{h|_{z=\eta_h^n}}^{n,\text{hor}} \cdot \nabla \eta_h^n\|_{0,\omega} \right]$$

$$+ \Delta t \left| s_h^n(\eta_h^n, \eta_h^{n+1} - \eta_h^n) \right| . \tag{88}$$

We next bound the terms on the right-hand side of (88). The norm of the convective derivative is linked to the stabilisation term as follows:

$$\|\boldsymbol{u}^{n,\mathrm{hor}}_{h|_{z=\eta^n_h}} \cdot \nabla \eta^n_h\|^2_{0,\omega} = \frac{\|\boldsymbol{u}^{n,\mathrm{hor}}_{h|_{z=\eta^n_h}}\|_{\infty,\omega}}{\mathfrak{h}}\, s^n_h(\eta^n_h,\eta^n_h) = \frac{\|\boldsymbol{u}^{n,\mathrm{hor}}_{h|_{z=\eta^n_h}}\|_{\infty,\omega}}{\mathfrak{h}}\, |\eta^n_h|^2_s. \tag{89}$$

Replacing (89) in (88) leads to

$$\begin{aligned}\|\eta^{n+1}_h - \eta^n_h\|^2_{0,\omega} \leq & \Delta t\, \|\eta^{n+1}_h - \eta^n_h\|_{0,\omega} \left[\|w^n_{h|_{z=\eta^n_h}}\|_{0,\omega} + \frac{\left\|\boldsymbol{u}^{n,\mathrm{hor}}_{h|_{z=\eta^n_h}}\right\|^{\frac12}_{\infty,\omega}}{\mathfrak{h}^{\frac12}}\, |\eta^n_h|_s\right] \\ & + \Delta t\, \left|s^n_h(\eta^n_h, \eta^{n+1}_h - \eta^n_h)\right|. \end{aligned} \tag{90}$$

It only remains to bound the stabilization term $s^n_h(\eta^n_h, \eta^{n+1}_h - \eta^n_h)$. Since $s^n_h(\cdot,\cdot)$ is symmetric we can use Cauchy-Schwarz's inequality and obtain

$$\begin{aligned} s^n_h(\eta^n_h, \eta^{n+1}_h - \eta^n_h) &\leq s^n_h(\eta^n_h,\eta^n_h)^{\frac12}\; s^n_h(\eta^{n+1}_h - \eta^n_h, \eta^{n+1}_h - \eta^n_h)^{\frac12} \\ &\leq \frac{\mathfrak{h}^{\frac12}}{\left\|\boldsymbol{u}^{n,\mathrm{hor}}_{h|_{z=\eta^n_h}}\right\|^{\frac12}_{\infty,\omega}}\, |\eta^n_h|_s\; \|\boldsymbol{u}^{n,\mathrm{hor}}_{h|_{z=\eta^n_h}} \cdot \nabla(\eta^{n+1}_h - \eta^n_h)\|_{0,\omega}, \end{aligned} \tag{91}$$

and then:

$$s^n_h(\eta^n_h, \eta^{n+1}_h - \eta^n_h) \leq \mathfrak{h}^{\frac12}\; |\eta^n_h|_s\; \|\boldsymbol{u}^{n,\mathrm{hor}}_{h|_{z=\eta^n_h}}\|^{\frac12}_{\infty,\omega}\; \|\nabla(\eta^{n+1}_h - \eta^n_h)\|_{0,\omega}. \tag{92}$$

Using the inverse inequality (85) on (92) yields:

$$s^n_h(\eta^n_h, \eta^{n+1}_h - \eta^n_h) \leq c_{inv}\; \mathfrak{h}^{-\frac12}\; |\eta^n_h|_s\; \left\|\boldsymbol{u}^{n,\mathrm{hor}}_{h|_{z=\eta^n_h}}\right\|^{\frac12}_{\infty,\omega} \|\eta^{n+1}_h - \eta^n_h\|_{0,\omega}. \tag{93}$$

We insert (93) in (90) and we have:

$$\begin{aligned}\|\eta^{n+1}_h - \eta^n_h\|^2_{0,\omega} \leq & \Delta t\, \|\eta^{n+1}_h - \eta^n_h\|_{0,\omega} \Big[\|w^n_{h|_{z=\eta^n_h}}\|_{0,\omega} \\ & + \mathfrak{h}^{-\frac12}\, |\eta^n_h|_s \left[\|\boldsymbol{u}^{n,\mathrm{hor}}_{h|_{z=\eta^n_h}}\|^{\frac12}_{\infty,\omega} + c_{\mathrm{inv}}\, \|\boldsymbol{u}^{n,\mathrm{hor}}_{h|_{z=\eta^n_h}}\|^{\frac12}_{\infty,\omega}\right]\Big]. \end{aligned} \tag{94}$$

Dividing by $\|\eta^{n+1}_h - \eta^n_h\|_{0,\omega}$ and squaring yields

$$\begin{aligned}\|\eta^{n+1}_h - \eta^n_h\|^2_{0,\omega} &\leq \Delta t^2 \left[2\, \|w^n_{h|_{z=\eta^n_h}}\|^2_{0,\omega} + 2\, \mathfrak{h}^{-1}\, |\eta^n_h|^2_s\, \|\boldsymbol{u}^{n,\mathrm{hor}}_{h|_{z=\eta^n_h}}\|_{\infty,\omega} \left[1 + c_{\mathrm{inv}}\right]^2\right] \\ &\leq 2\, \Delta t \left[\Delta t \|w^n_{h|_{z=\eta^n_h}}\|^2_{0,\omega} + 2\, \frac{\Delta t}{\mathfrak{h}}\, |\eta^n_h|^2_s\, \|\boldsymbol{u}^{n,\mathrm{hor}}_{h|_{z=\eta^n_h}}\|_{\infty,\omega} \big[1 + c^2_{\mathrm{inv}}\big]\right]. \end{aligned}$$

Hence, an application of the CFL condition (83) and the hypothesis on the size of α_0 conclude the proof. □

We finish this section by the main stability result concerning the free surface.

Theorem 3.11. *Let us suppose that* (83) *and* (84) *are satisfied, and let* $\eta^n_h \in \mathcal{N}_{\mathfrak{h}}(\omega)$ *be the solution of* (56)*. Then, for all* $m \in \{0, \ldots, N\}$ *the following stability bound holds: There exists* $C > 0$*, independent of* h*,* Δt*, and* m*, such that*

$$\|\eta^m_h\|^2_{0,\omega} + \Delta t \sum_{n=1}^{m-1} s^n_h(\eta^n_h,\eta^n_h) \leq \|\eta^0_h\|^2_{0,\omega} + \left(C + |\Omega^0_h|\right) T + T e^{2T} \left(\|\boldsymbol{u}^0_h\|^2_{0,0} + g^2 T\, |\Omega^0_h|\right). \tag{95}$$

Proof. Taking $\zeta_h = \eta^n_h$ in (56) and using that $-\boldsymbol{u}^{n,\mathrm{hor}}_{h|_{z=\eta^n_h}} \cdot \nabla \eta^n_h + w^n_h = \boldsymbol{u}^n_h \cdot \boldsymbol{n}^n_{h,s}$ on the free surface we get

$$\|\eta^{n+1}_h\|^2_{0,\omega} - \|\eta^n_h\|^2_{0,\omega} + 2\, \Delta t\, s^n_h(\eta^n_h,\eta^n_h) = 2\, \Delta t\, \left(\boldsymbol{u}^n_h \cdot \boldsymbol{n}^n_{h,s}, \eta^n_h\right)_\omega + \|\eta^{n+1}_h - \eta^n_h\|^2_{0,\omega}. \tag{96}$$

We develop each term in the right-hand side of the last equality. Changing variables it can be seen that

$$\big(\boldsymbol{u}_h^n \cdot \boldsymbol{n}_{h,s}^n, \eta_h^n\big)_\omega = \int_{\Gamma_{h,s}^n} \boldsymbol{u}_h^n \cdot \frac{\boldsymbol{n}_{h,s}^n}{\|\boldsymbol{n}_{h,s}^n\|} \eta_h^n \mathrm{d}\Gamma_{h,s}^n \,. \tag{97}$$

Using that $\eta_h^n|_{\Gamma_{h,s}^n} = z$, Green's formula, the fact that $\boldsymbol{u}_h^n$ satisfies (59) and that $z \in \mathcal{Q}_h(\Omega_h^n)$, the conservation of the water quantity, and Young's inequality, we get

$$\begin{aligned}
\big(\boldsymbol{u}_h^n \cdot \boldsymbol{n}_{h,s}^n, \eta_h^n\big)_\omega &= \int_{\partial\Omega_h^n} z\, \boldsymbol{u}_h^n \cdot \boldsymbol{n}\, \mathrm{d}\Gamma_{h,s}^n \\
&= \underbrace{\int_{\Omega_h^n} z \,\mathrm{div}\, \boldsymbol{u}_h^n \mathrm{d}\boldsymbol{x}}_{=0} + \int_{\Omega_h^n} \nabla z \cdot \boldsymbol{u}_h^n \mathrm{d}\boldsymbol{x} \\
&= \int_{\Omega_h^n} w_h^n \mathrm{d}\boldsymbol{x} \\
&\leq |\Omega_h^n|^{\frac{1}{2}} \|w_h^n\|_{0,\Omega_h^n} \\
&\leq \frac{1}{2}\,|\Omega_h^0| + \frac{1}{2}\,\|w_h^n\|_{0,\Omega_h^n}^2 \,. \qquad (98)
\end{aligned}$$

Next, to bound the other term on the right-hand side of (96), we start using the CFL conditions (83) and (84) to reach the following bound:

$$2\Delta t^2 \|w^n_{h|_{z=\eta_h^n}}\|_{0,\omega}^2 \leq 2\Delta t^2 \|w^n_{h|_{z=\eta_h^n}}\|_{\infty,\omega}^2 |\omega| \leq 2\alpha_0^2\,|\omega|\,h^2 \leq C\,\Delta t \,. \tag{99}$$

Inserting this last bound in Lemma 3.10 we arrive at

$$\|\eta_h^{n+1} - \eta_h^n\|_{0,\omega}^2 \leq \Delta t \left\{C + s_h^n(\eta_h^n, \eta_h^n)\right\}, \tag{100}$$

where the constant $C > 0$ does not depend on h, or Δt.

Thus, inserting (98) and (100) in (96) we obtain

$$\|\eta_h^{n+1}\|_{0,\omega}^2 - \|\eta_h^n\|_{0,\omega}^2 + \Delta t\, s_h^n(\eta_h^n, \eta_h^n) \leq \big(C + |\Omega_h^0|\big)\,\Delta t + \Delta t\,\|\boldsymbol{u}_h^n\|_{0,n}^2 \,, \tag{101}$$

and adding over $n = 0, \ldots, m-1$ we arrive at

$$\begin{aligned}
\|\eta_h^m\|_{0,\omega}^2 + \Delta t \sum_{n=0}^{m-1} s_h^n(\eta_h^n, \eta_h^n) &\leq \|\eta_h^0\|_{0,\omega}^2 + \big(C + |\Omega_h^0|\big)\,T + \Delta t \sum_{n=0}^{m-1} \|\boldsymbol{u}_h^n\|_{0,n}^2 \\
&\leq \|\eta_h^0\|_{0,\omega}^2 + \big(C + |\Omega_h^0|\big)\,T + T \max\{\|\boldsymbol{u}_h^n\|_{0,n}^2 : n = 0, \ldots, m-1\} \,. \qquad (102)
\end{aligned}$$

The proof is finished by applying Theorem 3.8 to bound the norm of the discrete velocity. □

Remark 3.12. *We finish this section by mentioning that restrictions on the mesh and time steps like* (84) *have appeared in the past, linked to the stability analysis of stabilised finite element methods for the Stokes and Navier-Stokes problems (see, e.g.,* [4, 5, 2]*).*

4. Numerical results

This section is devoted to test the performance of the present numerical strategy through some classical benchmarks. All the examples presented here involve a flat bottom and slip or no-slip boundary conditions on the bottom and on lateral boundaries. The first three examples are posed in a two-dimensional domain, and for them an analytical approximation of the solution is available. This approximation will be used as the reference, and the numerical solution will be compared to it. In addition, in the first example we compare our numerical results to those obtained using the approach presented in [23] and [9], which is based on a characteristics method in the ALE frame for the convection of the free surface (and the fluid velocity). The characteristics method is a well-established first order consistent method for the convection equation, whose numerical performance in the context of the free surface Navier-Stokes equations has been, so far, stable, although no rigorous proof of its stability is available, up to our best knowledge. However, as our numerical experiments also show, this characteristics method fails to preserve the total water

quantity, while the present method does. The second example is devoted to the propagation of a nonlinear soliton and the third one to a recirculation process. The final example presents a three dimensional application. In all the test cases, the time step is chosen in order to satisfy the CFL condition (83).

4.1. **Two-dimensional small amplitude water waves.** The first numerical test considers a sinusoidal free surface profile and a fluid at rest at the initial time. This test has been solved previously in, e.g., [9]. The density of the fluid is $\rho = 10^3 \mathrm{kg} \cdot \mathrm{m}^{-3}$ and the fluid is assumed to be inviscid; thus, the total energy is preserved and a continuous exchange of potential and kinetic energy takes place. The computational domain is a closed basin with side $L = 10\mathrm{m}$, equilibrium water depth $H = 10\mathrm{m}$ and constant bottom at $z = 0$. We denote by η_0 the amplitude of the initial wave (taken in this example to be $\eta_0 = 0.1\mathrm{m}$), and by $k = \pi/L$ its wave number. The initial free surface profile is then given by

$$\eta^0(x) = H + \eta_0 \cos(kx).$$

In this case the small amplitude wave theory for the linearized equations provides an accurate approximation of the solution – see for instance [6]. It is defined as follows:

$$\left\{ \begin{array}{rcl} \eta(t,x) = & H + \eta_0 \ \cos(kx) \ \cos(\omega t), \\ u(t,x,z) & = & \omega \ \eta_0 \ \frac{\cosh(kz)}{\sinh(kH)} \ \sin(kx) \ \sin(\omega t), \\ w(t,x,z) & = & -\omega \ \eta_0 \ \frac{\sinh(kz)}{\sinh(kH)} \ \cos(kx) \ \sin(\omega t), \end{array} \right. \tag{103}$$

with the dispersion relation $\omega^2 = g\,k \tanh(kH)$. The space step is taken equal to 1m and 0.1m, and for each of these spatial resolutions, the time step is respectively equal to 0.2s and 0.02s.

Figure 1 depicts the time evolution of a point of the free surface (at abscissa $x = 0$) computed with the current method and the method based on characteristics, both compared to the reference solution given by (103) for the two different space/time meshes. For the coarse mesh (figure on the left), we observe different behaviors for the current and the characteristic methods. The period of the oscillations is relatively well captured by both methods, even if it is slightly shortened for the characteristic method. But the amplitude of the oscillations is quite different : for the current method, one observes a noticeable but classical decreasing linked to the numerical diffusion of the method whereas for the characteristic method one first observes an increasing of the amplitude of the oscillations (and then of the potential energy) which then slightly decreases with time. When considering a refined mesh, both methods give very similar results and are in good agreement with the linearized solution.

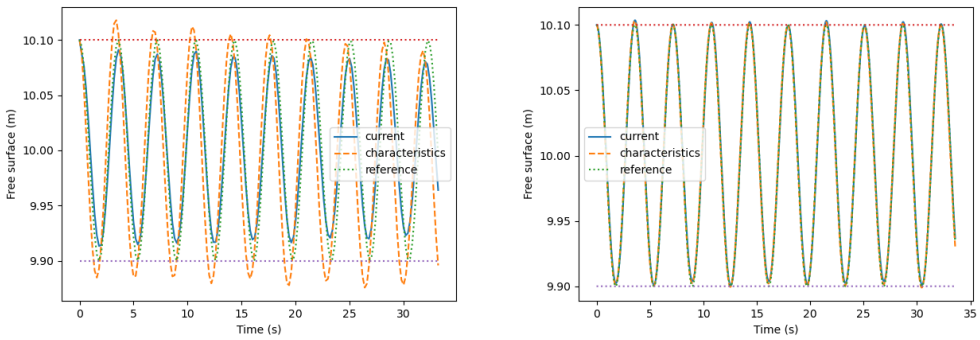

FIGURE 1. Time evolution of the computed free surface at $x = 0\mathrm{m}$ for $\Delta t = 0.2$ (left) and $\Delta t = 0.02$ (right).

To showcase the conservativity of the present method we define the relative mass loss of the fluid as follows

$$\Delta M(t) \;=\; \frac{\int_\omega (\eta(x,t))\mathrm{d}x}{\int_\omega \eta(x,0)\mathrm{d}x}.$$

Figure 2 shows the relative mass loss during the simulations, where we can observe that, while the present method preserves the mass up to machine precision, the characteristics method presents a loss of mass that continuously increases in time (although, as expected, this loss of mass decreases as the mesh and time steps get finer).

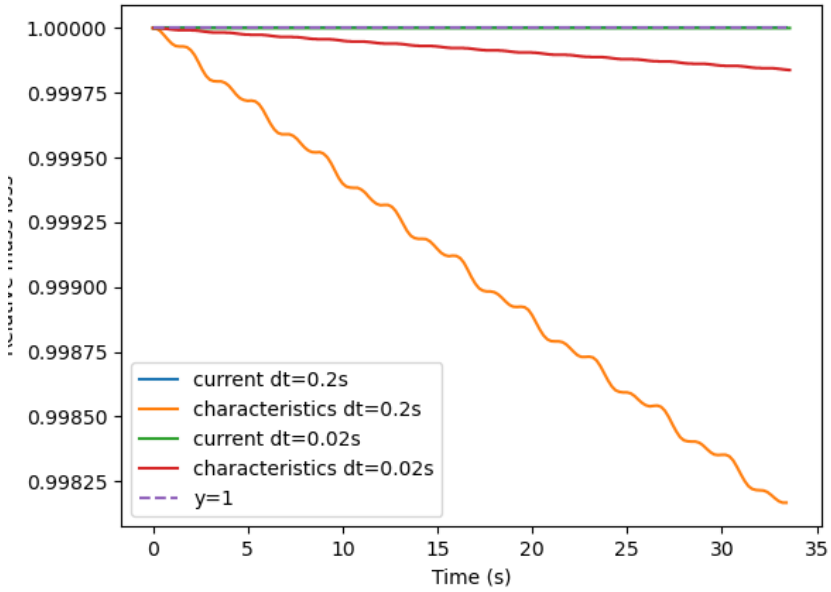

FIGURE 2. Time evolution of the computed relative total mass loss.

4.2. **Two-dimensional solitary wave.** The second numerical test considers a non linear wave that propagates on flat bottom from left to right without deformation, see [36]. The computational domain is a closed basin with length $L = 600\mathrm{m}$, equilibrium water depth $H = 10\mathrm{m}$ and constant bottom at $z = -10\mathrm{m}$. The density of the fluid is $\rho = 10^3 \mathrm{kg}\cdot\mathrm{m}^{-3}$ and the fluid is assumed to be non viscous. For moderate amplitude waves, an approximated solution is available, see [20]. This hydrostatic approximation of the velocity (u, w) and free surface η reads

$$\begin{aligned}
u(t,x) &= \sqrt{gH}\frac{\eta_0}{H}\,\mathrm{sech}^2\left(\sqrt{\frac{3}{4}\frac{\eta_0}{H^3}}(x-ct)\right)\\
\eta(t,x) &= H\left(1+\frac{u(t,x)}{\sqrt{gh}}\right),\\
w(t,x,z) &= \sqrt{3gH}\sqrt{\frac{\eta_0}{H}}\frac{z+H}{H}\,\mathrm{sech}^2\left(\sqrt{\frac{3}{4}\frac{\eta_0}{H^3}}(x-ct)\right)\tanh^2\left(\sqrt{\frac{3}{4}\frac{\eta_0}{H^3}}(x-ct)\right),\\
c &= \sqrt{g(H+\eta_0)},
\end{aligned}$$

where $g = 9.81\mathrm{m}\cdot\mathrm{s}^{-2}$ and $\eta_0 = 1\mathrm{m}$.

We approximate this problem using a space step equal to 1m and a time step equal to 6×10^{-2}s. In Figure 3 we compare our computed solution with this analytical approximated solution at times

$t = 12s$ and $t = 24s$. We observe a good agreement for the position and the amplitude of the soliton. Some small spurious oscillations are visible on the wake of the soliton wave. It is worth mentioning that such oscillations also appear in the solution for other numerical methods for this problem; for example, numerical experiments for using the characteristcs method (not reported here), also show similar oscillations.

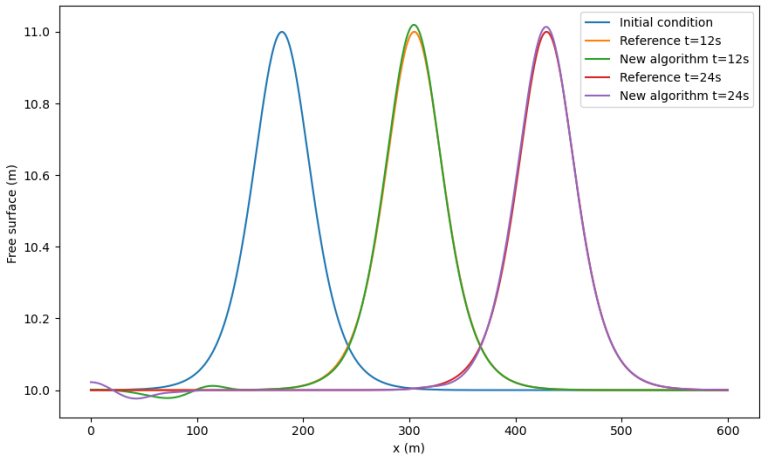

FIGURE 3. Computed free surface and position of the computed soliton at different times.

4.3. **Wind induced circulation.** The third numerical test considers the flow induced by wind blowing at the surface of a closed channel, see [36]. The computational domain is a rectangular channel with length $L = 6$m, equilibrium water depth $H = 10$m and constant bottom at $z = 0$m. The fluid is viscous with a kinematic viscosity coefficient $\mu = 10m^2s^{-1}$, and its density is $\rho = 1029\text{kg.m}^{-3}$. On the lateral boundaries, we consider slip boundary conditions, while on the bottom a no-slip condition $\boldsymbol{u} = \mathbf{0}$ is imposed. The flow is initially at rest. At the initial time, the channel is submitted to a constant wind with (horizontal) velocity $u_w = 1m.s^{-1}$. The force due to the wind is computed with the formula

$$\tau_w = \rho_a K \|u_w\| u_w, \qquad K = 0.05.$$

For this example we have considered a space step equal to 0.1m and a time step equal to 0.03s. In the left pannel of Figure 4 we depict the evolution of the free surface through time, where we can observe that the fluid reaches a steady-state recirculation, which is depicted in its right pannel. In the cross-section $x = 3$m, a semi-analytical approximation of the horizontal velocity can be found in [32], and is given by

$$u(z) = \frac{\tau_w H}{\rho \nu}(3z^2 - 4z + 1)\,. \tag{104}$$

This semi-analytical approximation is used as a target for comparison. In Figure 5 we depict the numerical solution and the approximation given by (104), where we can see that both are in good agreement.

4.4. **Three dimensional wave separation.** The final test case considered in this paper corresponds to the propagation and the reflection of water waves in a three-dimensional closed basin (see e.g. [9]). We consider a square basin with side $L = 10$m and with a water depth at the rest

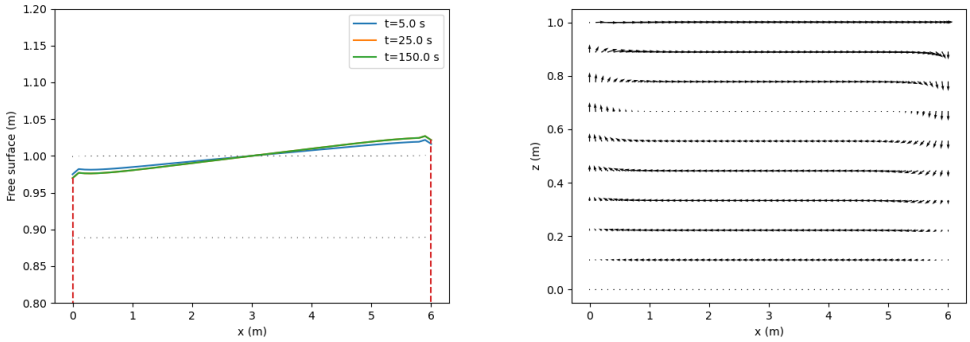

FIGURE 4. Computed free surface at different times (left) and velocity field at $t = 150$s (right).

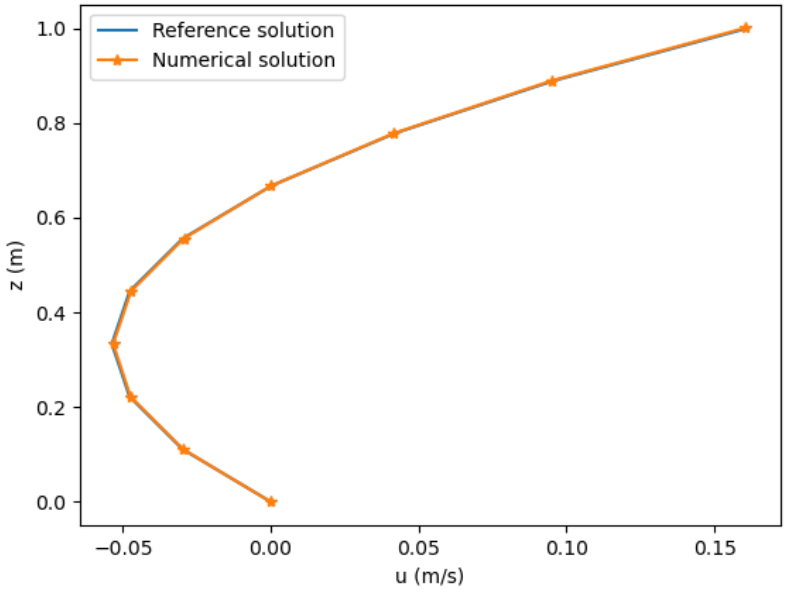

FIGURE 5. Vertical profile of the horizontal velocity at the center of the domain

$H = 1$m. The basin is filled by a fluid whose the initial free surface is the Gaussian shape function of amplitude $\eta_0 = 0.5$m given by:

$$\eta(x,0) = H + \eta_0 \exp\Big[-0.5\Big(x - \frac{L}{2}\Big)^2\Big]. \tag{105}$$

The peak of the Gaussian function is initially located at the center of the two-dimensional domain ω. We assume a flat bottom located at $z = -H$. At the initial time, the velocity field is assumed to be zero. The density and the viscosity of the fluid are respectively $\rho = 10^3 \text{kg} \cdot \text{m}^{-3}$ and $\mu = 10^{-1} \text{kg} \cdot (\text{m} \cdot \text{s})^{-1}$. Under the influence of the gravity, water waves are created and propagate to the extrema of the basin. At time $t \approx 3$s, the water waves reflect against the side walls and go back to the center of the basin.

The simulation of the propagation of the water wave is performed over $T = 10$s. The reference mesh $\widehat{\mathcal{T}}_h^{3D}$ is built by choosing the horizontal space step $\mathfrak{h}$ and the vertical one Δz equal to 0.25m.

The mesh $\{\mathcal{T}_h^{n,3D}\}_{n=0,\cdots,T}$ is built by distributing the vertical layers of $\widehat{\mathcal{T}}_h^{3D}$ using the ALE-Sigma transformation. The time step is chosen equal to $\Delta t = 0.02$s. In Figure 6 we depict snapshots of the free surface at different times, where it can be observed the reflection of the free surface once it has reached the boundary of the domain. Finally, in Figure 7 we present the time evolution of the position of the free surface at the center of the bassin for quantitative comparisons.

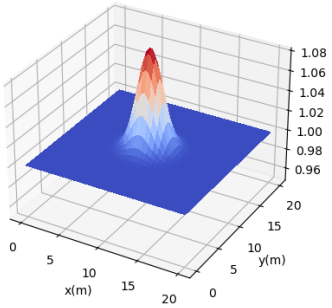

Initial configuration

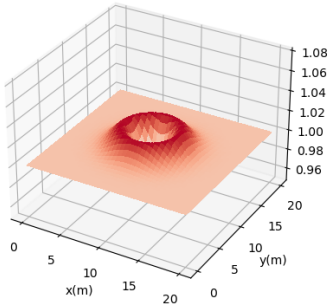

At time $t = 1$.s

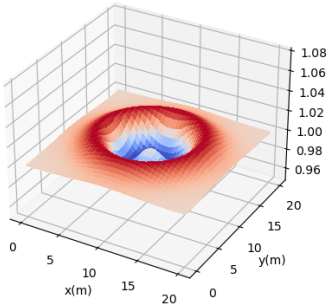

At time $t = 2$.s

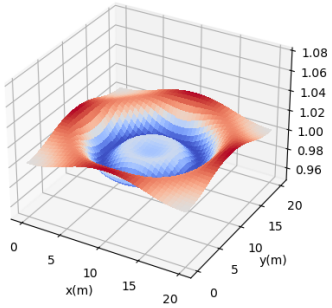

At time $t = 3$.s

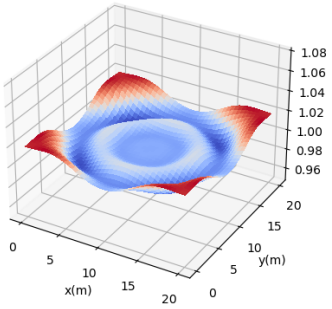

At time $t = 4$.s

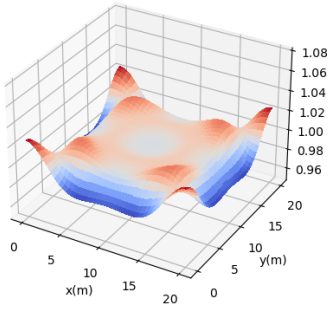

At time $t = 5$.s

FIGURE 6. Free surface at different times

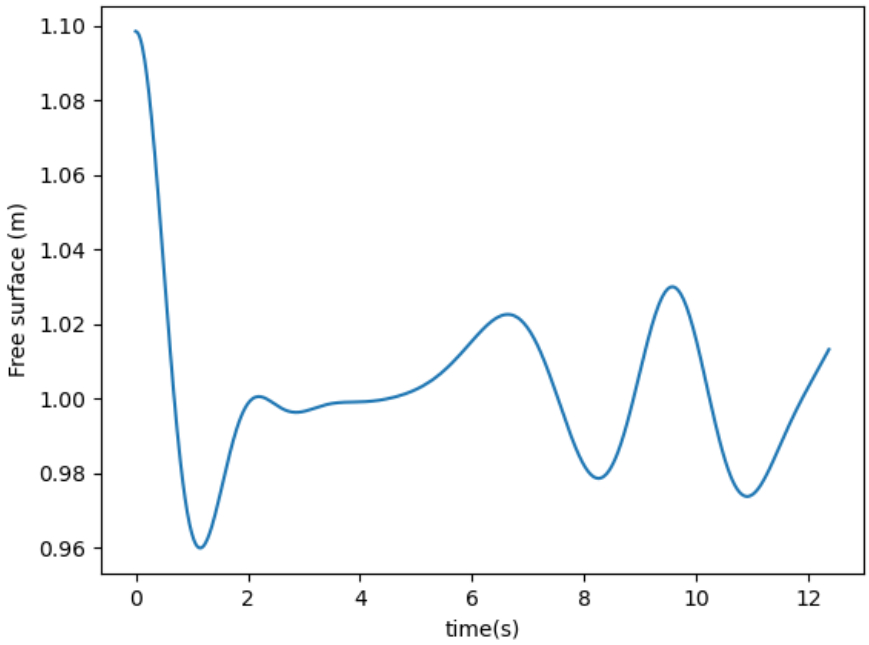

FIGURE 7. Time evolution of the computed free surface at the center of the bassin

ACKNOWLEDGEMENTS

Large portions of this work have been carried out during the stays of GRB at the Laboratoire LAGA. The financial support of Université Paris 13 is greatly acknowledged. The work of GRB has also being partially funded by the Leverhulme Trust through the Research Fellowship RF-2019-510. The work of PQ has been supported by EDF-LNHE and ANRT through the funding of his CIFRE PhD thesis.

REFERENCES

[1] Eberhard Bänsch. Finite element discretization of the Navier–Stokes equations with a free capillary surface. *Numerische Mathematik*, 88(2):203–235, 2001.

[2] Gabriel R. Barrenechea and Jordi Blasco. Pressure stabilization of finite element approximations of time-dependent incompressible flow problems. *Computer Methods in Applied Mechanics and Engineering*, 197(1):219–231, 2007.

[3] James Thomas Beale. Large-time regularity of viscous surface waves. *Archive for Rational Mechanics and Analysis*, 84(4):307–352, 1984.

[4] Jordi Blasco and Ramón Codina. Space and time error estimates for a first order, pressure stabilized finite element method for the incompressible Navier–Stokes equations. *Applied Numerical Mathematics*, 38(4):475–497, 2001.

[5] Pavel B. Bochev, Max D. Gunzburger, and John N. Shadid. On inf–sup stabilized finite element methods for transient problems. *Computer Methods in Applied Mechanics and Engineering*, 193(15):1471–1489, 2004.

[6] Robert G. Dean and Robert A Dalrymple. *Water wave mechanics for engineers and scientists*, volume 2. World Scientific Publishing Company, 1991.

[7] Astrid Decoene. *Hydrostatic model for three-dimensional free surface flows and numerical schemes*. PhD thesis, Université Pierre et Marie Curie - Paris VI; Laboratoire Jacques-Louis Lions, 2006.

[8] Astrid Decoene and Jean-Frédéric Gerbeau. Sigma transformation and ALE formulation for three-dimensional free surface flows. *International Journal for Numerical Methods in Fluids*, 59(4):357–386, 2009.

[9] Astrid Decoene and Bertrand Maury. Moving meshes with freefem++. *Journal of Numerical Mathematics*, 20(3-4):195–214, 2012.

[10] Fabián Duarte, Raúl Gormaz, and Srinivasan Natesan. Arbitrary lagrangian–eulerian method for Navier–Stokes equations with moving boundaries. *Computer Methods in Applied Mechanics and Engineering*, 193(45):4819–4836, 2004.
[11] Alexandre Ern and Jean-Luc Guermond. *Finite elements I—Approximation and interpolation*, volume 72 of *Texts in Applied Mathematics*. Springer, Cham, 2021.
[12] Deepak Garg, Antonella Longo, and Paolo Papale. Modeling free surface flows using stabilized finite element method. *Mathematical Problems in Engineering*, 2018:Article ID 6154251, 9 pages, 2018.
[13] Pilip H. Gaskell, M. D. Savage, Jonathan L. Summers, and Harvey M. Thompson. Modelling and analysis of meniscus roll coating. *Journal of Fluid Mechanics*, 298:113–137, 1995.
[14] Jean-Frédéric Gerbeau, Tony Lelièvre, and Claude Le Bris. Simulations of mhd flows with moving interfaces. *Journal of Computational Physics*, 184(1):163–191, 2003.
[15] Vivette Girault and Pierre-Arnaud Raviart. *Finite element methods for Navier-Stokes equations. Theory and algorithms.*, volume 5 of *Springer Series in Computational Mathematics*. Springer-Verlag, Berlin, 1986.
[16] Yan Guo and Ian Time. Local well-posedness of the viscous surface wave problem without surface tension. *Analysis and PDEs*, 6(2):287–369, 2013.
[17] Jean Michel Hervouet. *Hydrodynamics of free surface flows, modelling with finite element method*. John Wiley & Sons Ltd., 2007.
[18] John G. Heywood and Rolf Rannacher. Finite-element approximation of the nonstationary Navier-Stokes problem. IV. Error analysis for second-order time discretization. *SIAM J. Numer. Anal.*, 27(2):353–384, 1990.
[19] Cyril W. Hirt, Anthony A. Amsden, and J.L. Cook. An arbitrary Lagrangian-Eulerian computing method for all flow speeds. *Journal of Computational Physics*, 14(3):227–253, 1974.
[20] Edmund V. Laitone. The second approximation to cnoidal and solitary waves. *Journal of Fluid Mechanics*, 9:430–444, 1960.
[21] Ching-Long Lin, Haegyun Lee, Taehun Lee, and Larry J. Weber. A level set characteristic galerkin finite element method for free surface flows. *International Journal for Numerical Methods in Fluids*, 49(5):521–547, 2005.
[22] Nader Masmoudi and Frédéric Rousset. Uniform regularity and vanishing viscosity limit for the free surface Navier–Stokes equations. *Archive for Rational Mechanics and Analysis*, 223(1):301–417, 2017.
[23] Bertrand Maury. Characteristics ale method for the unsteady 3d Navier–Stokes equations with a free surface. *International Journal of Computational Fluid Dynamics*, 6(3):175–188, 1996.
[24] Fabio Nobile and Luca Formaggia. A stability analysis for the arbitrary lagrangian eulerian formulation with finite elements. *East-West Journal of Numerical Mathematics*, 7(2):105–132, 1999.
[25] Norman A. Phillips. A coordinate system having some special advantages for numerical forecasting. *J Meteorol*, 14:184–185, 1957.
[26] Marco Picasso, Jacques Rappaz, Adrian Reist, Martin Funk, and Heinz Blatter. Numerical simulation of the motion of a two-dimensional glacier. *International Journal for Numerical Methods in Engineering*, 60(5):995–1009, 2004.
[27] Stéphane Popinet and Stéphane Zaleski. A front-tracking algorithm for accurate representation of surface tension. *International Journal for Numerical Methods in Fluids*, 30(6):775–793, 1999.
[28] Osborne Reynolds, Arthur W. Brightmore, and William H. Moorby. *Papers on Mechanical and Physical Subjects: The sub-mechanics of the universe, vol. 3.* The University Press, 1903.
[29] Jorge San Martín, Loredana Smaranda, and Takéo Takahashi. Convergence of a finite element/ale method for the stokes equations in a domain depending on time. *Journal of Computational and Applied Mathematics*, 230(2):521–545, 2009.
[30] Josep Sarrate, Antonio Huerta, and Jean Donea. Arbitrary lagrangian-eulerian formulation for fluid–rigid body interaction. *Computer Methods in Applied Mechanics and Engineering*, 190:3171–3188, 2001.
[31] Alfred Schmidt. Computation of three dimensional dendrites with finite elements. *Journal of Computational Physics*, 125(2):293–312, 1996.
[32] Nilakantan J. Shankar, Hinfatt F. Cheong, and Seetharaman Sankaranarayanan. Multilevel finite-difference model for three-dimensional hydrodynamic circulation. *Ocean Engineering*, 24(9):785–816, 1997.
[33] Alexander F. Shchepetkin and James C. McWilliams. The regional ocean model system (ROMS): A split-explicit, free-surface, topography-following coordinate ocean model. *Ocean Modelling*, 9:347–404, 2005.
[34] Satoshi Tanaka and Kazumi Kashiyama. Ale finite element method for fsi problems with free surface using mesh re-generation method based on background mesh. *International Journal of Computational Fluid Dynamics*, 20(3-4):229–236, 2006.
[35] Atusi Tani. Small-time existence for the three-dimensional Navier-Stokes equations for an incompressible fluid with a free surface. *Archive for Rational Mechanics and Analysis*, 133(4):299–331, 1996.
[36] Consortium Telemac-Mascaret. Telemac 3d : Validation manual. Technical report, http://wiki.opentelemac.org/, 2021.
[37] Mark A. Walkley, Pilip H. Gaskell, Peter K. Jimack, Mark A. Kelmanson, Jon L. Summers, and Mark C. T. Wilson. On the calculation of normals in free-surface flow problems. *Communications in Numerical Methods in Engineering*, 20(5):343–351, 2004.

Laboratoire Analyse, Géométrie et Applications (LAGA), Institut Galilée, Université Sorbonne Paris Nord, 99 avenue J.B. Clément 93430 Villetaneuse, France
Email address: audusse@math.univ-paris13.fr

Department of Mathematics and Statistics, University of Strathclyde, 26 Richmond Street, Glasgow, G1 1XH United Kingdom
Email address: gabriel.barrenechea@strath.ac.uk

Institut de Mathématiques de Bordeaux UMR 5251 Université de Bordeaux 351, cours de la Libération - F 33 405 TALENCE
Email address: astrid.decoene@u-bordeaux.fr

Laboratoire Analyse, Géométrie et Applications (LAGA), Institut Galilée, Université Sorbonne Paris Nord, 99 avenue J.B. Clément 93430 Villetaneuse, France
Email address: pierrick.quemar@gmail.com